Investigation of aging processes in bitumen at the molecular level with high resolution Fourier transform ion cyclotron mass spectrometry and two-dimensional gas chromatography mass spectrometry

Journal:	*Energy & Fuels*
Manuscript ID	ef-2020-01242e.R1
Manuscript Type:	Article
Date Submitted by the Author:	n/a
Complete List of Authors:	Neumann, Anika; University of Rostock, Joint Mass Spectrometry Centre, Chair of Analytical Chemistry Käfer, Uwe; Helmholtz Center Munich German Research Center for Environmental Health, Joint Mass Spectrometry Centre, Comprehensive Molecular Analytics Gröger, Thomas; Helmholtz Center Munich German Research Center for Environmental Health, Joint Mass Spectrometry Centre, Comprehensive Molecular Analytics Wilharm, Thomas; ASG Analytik-Service Gesellschaft mbH Zimmermann, Ralf; University of Rostock, Joint Mass Spectrometry Centre, Chair of Analytical Chemistry ; Helmholtz Center Munich German Research Center for Environmental Health, Joint Mass Spectrometry Centre, Comprehensive Molecular Analytics Rüger, Christopher; University of Rostock, Joint Mass Spectrometry Centre, Chair of Analytical Chemistry

Investigation of aging processes in bitumen at the molecular level with high resolution Fourier transform ion cyclotron mass spectrometry and two-dimensional gas chromatography mass spectrometry

Anika Neumann [1], Uwe Käfer [2], Thomas Gröger [2], Thomas Wilharm [3], Ralf Zimmermann [1,2], Christopher P. Rüger [1]

[1] Joint Mass Spectrometry Centre, Chair of Analytical Chemistry, University of Rostock, Dr. Lorenz-Weg 2, 18059 Rostock, Germany

[2] Joint Mass Spectrometry Centre, Comprehensive Molecular Analytics, Helmholtz Center Munich German Research Center for Environmental Health, Ingolstädter Landstr. 1, 85764, Neuherberg, Germany

[3] ASG Analytik-Service Gesellschaft mbH, Trentiner Ring 30, 86356, Neusäss, Germany

Abstract

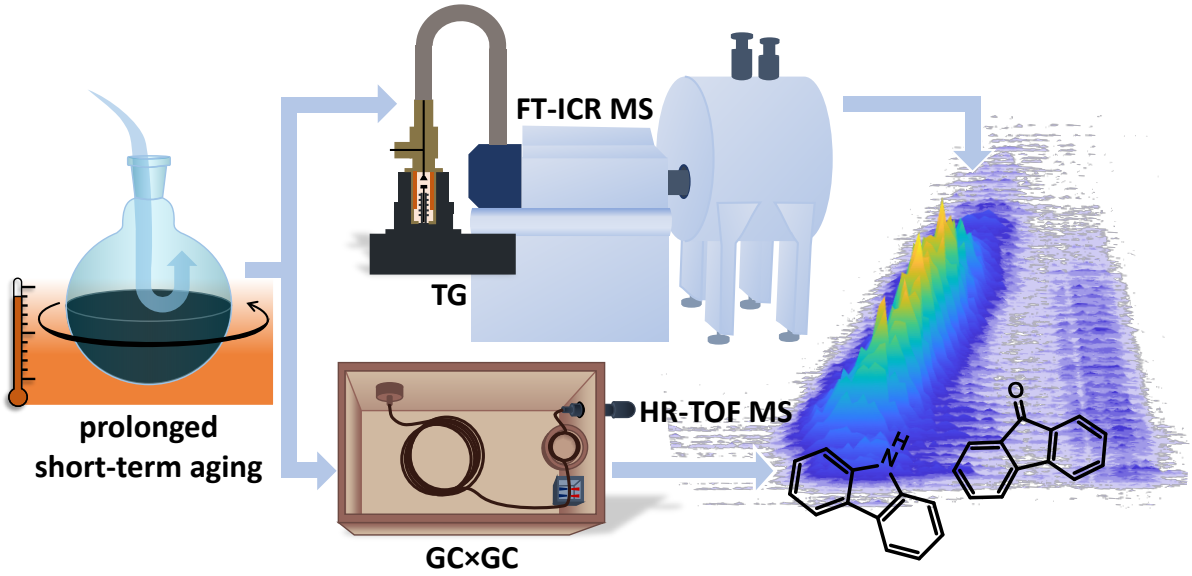

Bitumen is a highly viscous and chemically complex petroleum-derived material, which is applied as a binder in road construction. However, the asphalt underlies hardening, cracking, and embrittlement due to oxidative short-term aging during the mixing and paving process, but also due to long-term aging during the service time of the pavement.

In this study, chemical changes occurring during short-term aging, mimicked by a prolonged rotating flask procedure, are investigated for an artificial bitumen model at the molecular level. The model bitumen enables the application of two complementary analytical techniques for a comprehensive insight into the aging effects: high-resolution Fourier transform ion cyclotron mass spectrometry (FT-ICR MS) coupled to thermogravimetry (TG) was applied to investigate the aging effects on polar to semi-polar high molecular weight compounds ionized with atmospheric pressure chemical ionization (APCI). Aromatic core structures were analyzed by alternating collision-induced dissociation (CID). In order to support structural assignments from FT-ICR MS data in the semi-volatile region, comprehensive two-dimensional gas chromatography mass spectrometry (GC×GC-HRTOFMS) with electron ionization (EI) with 70 eV was applied for the group type analysis and the investigation of particular chemical functionalities.

Oxidation processes were revealed to be the prevalent reactions caused by short-term aging for the hydrocarbons (CH-class) and the sulfur-containing classes. Aromatic species with low steric hindrance or activated carbon positions as well as high aromatic core structures are favorably oxidized, forming carbonylic functionalities. For molecules with one sulfur-atom (S1-class), non-aromatic species like tetrahydrothiophenes decrease, whereas aromatic S1-compounds remain constant. Non-aromatic S1O1-species tend to further oxidation, while higher aromatic species occur with ongoing aging time. Moreover, this study highlights the aging behavior of nitrogen-containing compounds, such as carbazoles. A significant reduction of the N-classes was observed during aging, indicating thermal-induced condensation reactions as well as favored oxidation of highly aromatic core structures.

Introduction

Bitumen is a viscous, involatile, and highly complex mixture derived from petroleum vacuum residues or naturally occurring asphalt. It is composed of high-boiling molecules with high aromaticity as well as a high content of nitrogen, sulfur, and oxygen, which is present as functional groups like sulfides, pyridinic or pyrrolic type structures, phenolic compounds or carboxylic acids. [1,2] In road construction, bitumen is used as a binder for mineral aggregates to create asphalt concrete. Several modifiers, such as elastomers, plastomers, or crumb rubber, can be added to design and improve viscosity, elasticity, hardness, and the lifetime of the pavement [3–5]. During service time, the asphalt becomes more viscous, harder, brittle, and eventually cracked, which can be caused by the aging of the material. [6] The aging process can be divided into two different time ranges. First, short-term aging occurs during the mixing of the binder with the aggregates as well as the paving process and is characterized by high temperatures (150-160 °C) and a high specific surface of the bitumen mixture. Second, long-term aging appears during the service-time of the bitumen and is induced by climatic conditions, void content of the material, and oxidation. In laboratory studies, short term aging is simulated by the rolling thin film oven test (RTFOT) or rotating flask test (RFT), while long term aging is performed in a pressure aging vessel (PAV) and usually carried out after RTFOT-conditioning [7–12]. Different mechanisms lead to altered characteristics of the bitumen caused by the aging process. Besides the evaporation of low volatile species, the phase separation of bitumen compounds, and the physical hardening due to molecular organization, the mechanism considered as most important is oxidative aging [13,14]. Oxidation causes hardening and embrittlement of the binder due to the formation of polar functional groups, such as sulfoxides, anhydrides, carboxylic acids, and carbonyls [1,2].

The effects of aging on bitumen are routinely investigated by the determination of physical properties, such as the penetration index [15,16] or rheological properties measured with dynamic shear rheometry (DSR) [9,17–21], which provide insights into mechanical characteristics. Aging typically results in hardening, a decrease in elasticity, and an increased viscosity. Due to the extreme complexity of bitumen, detailed chemical characterization of aging effects is still an analytical challenge, and therefore,

chemical analyses are mostly limited to functional group analysis or the fractionation in saturates, aromatics, resins, and asphaltenes (SARA fractionation) [22]. With infrared spectroscopy (IR), the formation of carbonyl as well as sulfoxide functions during oxidative aging is frequently reported in the literature [4,23–25]. It was shown that sulfoxides are formed with higher reaction rates than carbonyls, and moreover, a temperature dependence of the oxidation reaction was revealed [9,26–28]. SARA fractionation is used since the 1960s for the chemical description of bitumen [29]. Saturates are considered as almost inert with respect to oxidation [18,25], while resins and asphaltenes show stronger changes [4,25]. Petersen et al. (2009) ranked the reactivity of the SARA fractions with oxygen in the following order: saturates < aromatics < resins < asphaltenes, while the asphaltene fraction is the most reactive one[1] . Hofko et al. (2016) showed that the asphaltene content is strongly related to the rheological properties of bitumen [20]. Atomic force microscopy (AFM) reveals a micelle-like structure of asphaltenes surrounded by resin and polar aromatics molecules, and different aging studies showed an increase in resin- and asphaltene-structures over aging time [3,30,31]. Recently, Weigel et al. (2017) showed a modeling approach with which physical, rheological, and aging behavior could be derived from the SARA distribution [32]. Nonetheless, the molecular level of bitumen aging is still poorly understood. In 2017, Handle et al. demonstrated the potential of Fourier transform ion cyclotron resonance mass spectrometry (FT-ICR MS) to investigate the aging behavior of highly polar species in bituminous material [33]. In the last decades, FT-ICR MS provided, due to its high mass accuracy and ultra-high resolution, valuable insights in the field of petroleomics, and particularly in highly complex fractions such as asphaltenes or vacuum residues [34–39]. Besides typical spray-based sample introduction, the hyphenation to thermogravimetry (TG) already showed in different studies its value for the investigation of high boiling petroleum fractions [40,41]. For more volatile as well as less polar fractions, two-dimensional gas chromatography coupled to mass spectrometry (GC×GC-MS) is extensively used in the field of petroleomics to cope with the enormous complexity of petroleum-derived sample material [38,42–45]. Chromatographic separation in two orthogonal dimensions with subsequent mass spectrometric detection enables the separation of complex mixtures, identification

of resolved analytes, and the classification into chemical groups. However, due to the volatility limit of gas chromatographic techniques, GC×GC-MS is only applicable for the analysis of volatile to semi-volatile fractions. Combining the advantages of FT-ICR MS and GC×GC-MS was already shown to allow for a comprehensive description of several crude oils[46], petroleum cuts[47], and bio oils[48,49].

The aim of this study is the investigation of oxidative short-term aging of bitumen at the molecular level attempting a detailed understanding of the complex chemical processes. Identifying compounds, which are highly affected by aging, will help to design durable and long-living pavements. To focus on the aging effects in neat bitumen, an artificial bitumen model was generated without adding any modifiers and specifically designed to contain components in the boiling range of gas chromatographic application offering the opportunity of structural elucidation. The model bitumen was treated under prolonged short-term aging conditions to enhance chemical reactions triggered by high temperatures in the presence of oxygen and to allow for their detection. Multiple sampling during the aging procedure enables the tracing of aging-related chemical changes. The occurring effects were analyzed by atmospheric pressure chemical ionization (APCI) TG-FT-ICR MS and confirmed as well as partially complemented by electron ionization (EI) GC×GC-HRTOFMS. The application of TG-FT-ICR MS enables the attribution of sum formulae up to the highly complex heavy end of the model bitumen. Additionally, aromatic core structures were addressed by alternating collision-induced dissociation (CID). Heteroatom-containing minorities were highlighted by APCI, which selectively ionizes semi-polar to polar species [50,51]. The additional chromatographic analytical dimension of GC×GC-HRTOFMS is able to contribute structural information, which supports and confirms structural estimations of FT-ICR MS data, especially in the semi-volatile region. Because of the compositional continuum (Boduszynski model) known for crude oil-derived material [52–56], the results can, to a certain extent, be expanded to high-boiling regions. The universal ionization technique EI applied for GC×GC-HRTOFMS allows for a broad chemical description of the sample material including nonpolar hydrocarbons, which complements the smaller chemical space obtained by APCI for FT-ICR MS data. Within this study, a detailed description of short-term aging effects in the bitumen model was envisioned by the

combination of both techniques. Aging-related alterations are presented at the molecular level for different hydrocarbon classes, oxidized hydrocarbons as well as sulfur- and nitrogen-containing species and their corresponding oxidized representatives.

Materials and Methods

Sample Preparation

For the preparation of the model bitumen, a heavy crude oil (Mittelplate crude oil) with an API gravity of 21° was used. The volatile compounds (up to 200 °C) of the crude oil were removed by distillation in accordance with ASTM D2892 [57] using a 15-theoretical-plate batch distillation system (Pilodist 100, Pilodist, Merckenheim, Germany) to generate a controlled sample matrix without any chemical modifiers. Detailed information on the distillation procedure can be found elsewhere [43]. The remaining residue was aged with a modified rotating flask test for 168 h at 150°C under air atmosphere. In this setup, skin formation of the viscous sample is prevented by the constant rotation of the flask and continuous renewal of the sample surface is ensured. Moreover, in order to prevent depletion of oxygen in the atmosphere, a constant air flow of 2 L/min was maintained. The model bitumen was sampled after a 1 day (24 h), 2 days (48 h), 3 days (72 h), 4 days (96 h), and 7 days (168 h), respectively. Including the non-aged sample (0 days), a sample set containing six different aging stages was obtained, which enables a continuous, multi-stage description of chemical changes in the matrix.

Thermogravimetry Fourier Transform Ion Cyclotron Mass Spectrometry with Atmospheric Pressure Ionization (TG-APCI-FT-ICR MS)

Each of the bitumen samples representing different aging stages were measured by thermogravimetry (TG) coupled to atmospheric pressure chemical ionization (APCI) Fourier Transform ion cyclotron mass spectrometry (FT-ICR MS) in triplicates. The detailed description of the set-up can be found elsewhere[58]. The method was previously shown to reveal valuable information on high complex petroleum samples.[40,41] In short, approximately 1 mg of the samples were directly introduced in a single-use aluminum crucible to the thermobalance (TG 209 cell thermo balance, Netzsch, Selb, Germany). Under a constant flow of nitrogen of 200 ml/min, the sample was heated from 20 °C (held for 2 min) up to 600 °C (held for 10 min) with a heating rate of 10 K/min. 2 ml/min of the evolved gas mixture was transferred to the ionization chamber via a slight overpressure of 8 mbar over a heated transfer-line (deactivated fused silica capillary, 0.53 mm ID, 300 °C). The filled TG crucibles were weighed before and after the measurements to determine the residual masses, which are summarized in Table S1 for each measurement. Atmospheric pressure ionization was carried out in a GC-APCI II ion source (Bruker Daltonics, Bremen, Germany) using a current of 3,000 nA for corona discharge. Temperature resolved mass spectra were recorded on a 7 Tesla FT-ICR MS equipped with infinity cell (APEX Qe, Bruker Daltonics, Bremen, Germany) and a resolving power of 260,000 at *m/z* 400 resulting from 2 s transient. Every 10 seconds a broadband spectrum for *m/z* 100-1000 was recorded in MS-mode consisting of 5 microscans for enhancing the signal to noise ratio of low-abundant signals. Alternating MS/MS-mode was applied, *i.e.*, 5 microscans of the intact molecules were registered in turns with 5 microscans of fragmented molecules. This procedure allows to investigate the aromatic core structures of alkylated constituents [59,60]. For fragmentation, collision-induced dissociation (CID) was applied, using a collision voltage of 30 V and a higher accumulation time of 1 s.

Comprehensive time-resolved processing was carried out using Bruker DataAnalysis 5.1 for *m/z*-pre-calibration of the summed mass spectra and a self-written tool CERES based on in-house Matlab scripting (R2018b, 64-bit) for further processing (feature detection) and sum formula calculation (including evaluation and validation). Every measurement was internal linearly calibrated on homologues rows in DataAnalysis and again every single spectrum during processing in CERES to correct for frequency shifts resulted from varying ion loads in the FT-ICR MS cell. The elemental composition attribution was carried out for MS-spectra with the following restrictions: #C 6-70, #H 4-200, #N 0-1, #O 0-4, #S 0-2, H/C ratio 0-3, ring and double bond equivalent (DBE) 0-40, and a sum formula error of 1 ppm. For MS/MS-spectra, the following restriction were applied: #C 6-70, #H 4-200, #N 0-2, #O 0-2, #S 0-3, H/C ratio 0-3, DBE 0-40 as well as a sum formula error of 1 ppm. In Figure S1, the sum formula error distribution is given for non-aged model bitumen. In general, sum formulae could be attributed with a root mean square error below 0.28 ppm for MS-mode and below 0.31 ppm for MS/MS-mode.

Two-dimensional gas chromatography coupled to high-resolution time-of-flight mass spectrometry (GC×GC-HRTOFMS)

Samples were dissolved in dichloromethane (DCM)[61] (20 % wt) and 1 µL of the solution was injected using a programmable temperature vaporizing (PTV) unit (Optic 4, GL Science, Eindhoven, Netherlands). GC×GC experiments were conducted on a Leco Pegasus HRT 4D (Leco, St. Joseph, MI, USA) with an Agilent technologies 7890A gas chromatograph (Palo Alto, CA, USA). The system was equipped with a dual-stage liquid nitrogen thermal modulator and a secondary oven, placed inside the main GC oven. The GC method used for analyzing the model bitumen samples was already evaluated and applied for heavy fractions in earlier studies.[42,43,62,63] In brief, a high-temperature column combination consisting of a Phenomenex Zebron ZB-35HT Inferno (30 m × 0.25 mm; film: 0.1 µm) as

first dimension and a SGE BPX1 (1.5 m × 0.1 mm; film: 0.1 µm) as second dimension were used. The complete overview of instrumental parameters is presented in the supporting information in Table S2. Each sample was measured in triplicates to determine the methodological variance.

GC×GC–data was post-processed with ChromaTOF HRT (version 5.10, Leco, St. Joseph, MI, USA). Chromatograms were manually checked for the presence of chemical classes and subsequently detected peaks were classified by retention time regions and mass spectral filters to compound classes. Details about the classification procedure can be found in the literature [62,63]. Peak areas were normalized to the total ion current and summarized to compound classes to obtain the relative abundance of respective chemical groups.

Results and discussion

In the following, the aging effects observed with TG-FT-ICR MS supported by GC×GC-HRTOFMS are shortly discussed on a macroscopic level for generally observed alterations and in detail for three groups of compound classes at the molecular level. The components were divided in the hydrocarbon class (CH-class), sulfur-containing classes (S_x-class) as well as nitrogen-containing classes (N_x-class) and their corresponding oxidation products (O_x-class, S_xO_y-class, and N_xO_y-class), respectively. Aging-related trends were statistically validated at 95 % statistical certainty applying the WEIR t-test [64], which is especially designed for a limited number of replicates.

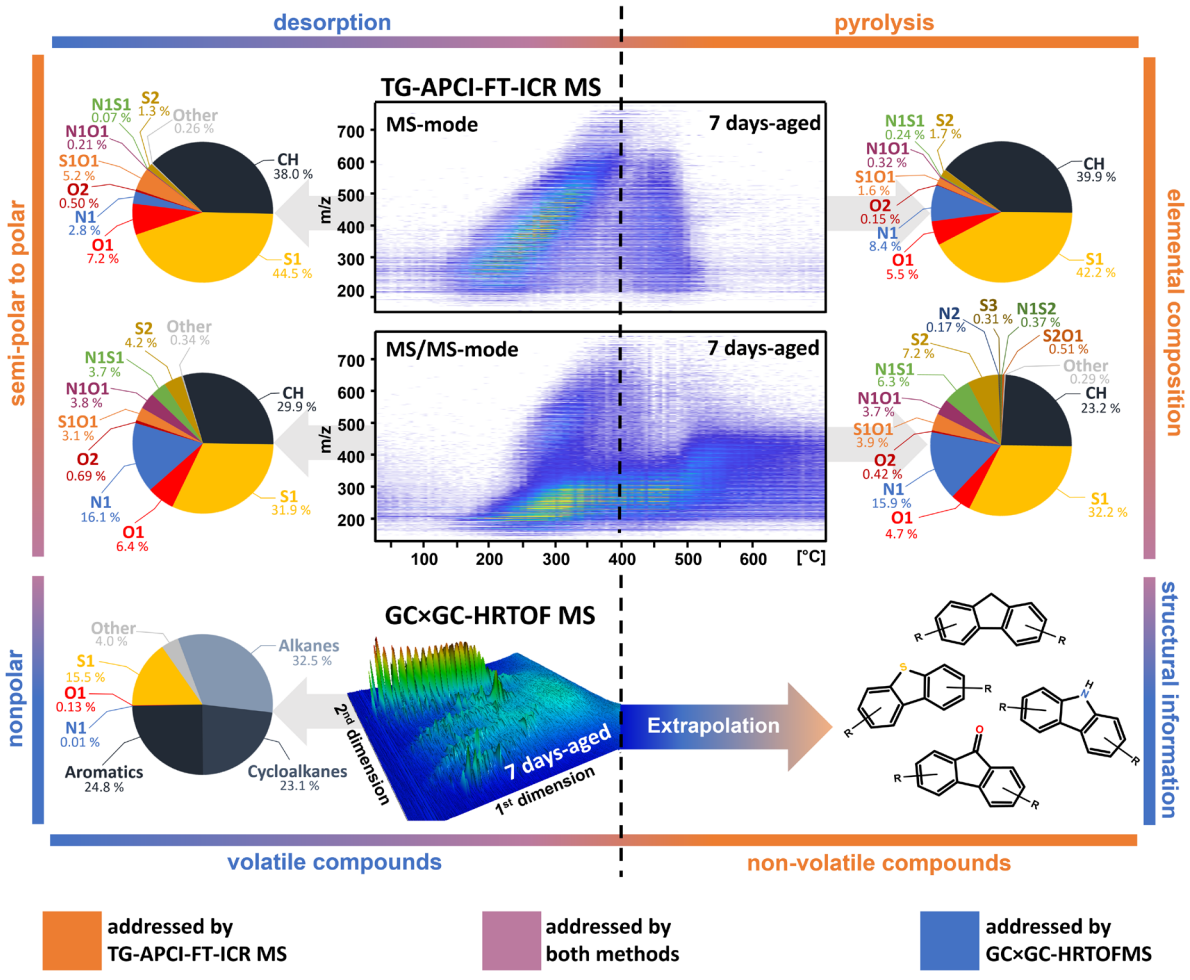

Figure 1: Method integration of TG-APCI-FT-ICR MS and GC×GC-HRTOFMS exemplarily depicted for 7 days-aged model bitumen. Desorbable and pyrolyzable species are separated at the dashed line. Pie charts on the left side correspond to the class distribution found for desorption, while pie charts on the right side give the class distribution for the pyrolysis phase. TG-APCI-FT-ICR MS is able to attribute sum formulae to semi-volatile to pyrolyzable compounds. Due to APCI, semi-polar to polar minorities are highlighted. The 2D survey view of the temperature-resolved mass spectra for MS-mode and MS/MS-mode color-coded with intensity shows the characteristic increase of the m/z with increasing temperature in the desorption phase, while an enlarged m/z range is simultaneously covered in the pyrolysis phase. GC×GC-HRTOFMS enables the structural

elucidation of volatile compounds. With electron ionization, non-polar compounds are covered as well. Two-dimensional gas chromatography allows for group-type analysis of volatile compounds up to roughly m/z 600.

Before discussing the observed aging effects, the capabilities of the applied techniques are introduced in more detail. Figure 1 illustrates the integration of the methodologies using the example of the 7 days-aged model bitumen. Additional temperature resolved FT-ICR MS mass spectra, as well as GC×GC-HRTOFMS chromatograms for the non-aged sample, are given in Figure S2 and Figure S3 of the supplemental material, respectively. Due to the thermogravimetric sample introduction under nitrogen atmosphere, TG-FT-ICR MS data can be divided into two phases attributable to temperature, which is visualized by the dashed line in Figure 1. From 100 to 400 °C, a desorption phase is observed, in which intact species up to *m/z* 750 are evaporated. In the second phase from 400 to 600 °C, pyrolysis occurs leading to a decomposition of high molecular weight species into smaller thermal fragments. In addition to the differentiation into desorption and pyrolysis phase of the FT-ICR MS data, collision-induced dissociation (CID) was applied during MS/MS-mode alternating with the recording of normal MS-spectra. Typically, when using CID under moderate conditions, aromatic compounds are partially dealkylated and the charge remains on the aromatic core. [59,60] Because of the mass loss due to dealkylation and enhanced ion storage time, smaller molecules and/or compounds with low ring and double bond equivalent (DBE) shift under the detectable mass limit of the FT-ICR MS and therefore, MS/MS-data give a slightly shifted view concerning *m/z* or DBE. On the other hand, valuable information is obtained on high-molecular species because of two mutual enhancing effects. First, due to longer accumulation times, also low abundant or only weakly ionized species could be detected, and second, a variety of compounds with different degrees of alkylation are fragmented to the same core structure also enhancing the intensity. FT-ICR MS was equipped with the soft ionization technique APCI resulting in the detection of preserved molecular ions and highlighting semi-polar to polar minorities. Figure 1 illustrates the class distributions as pie charts for desorption and pyrolysis phase to reveal the differences in relative intensity of the attributed classes between the different phases. In general, the pyrolysis phase exhibits a higher chemical diversity than the desorption phase,

which can be explained by the Boduszynski model [55]. In petroleum-derived material, high-boiling fractions exhibit a higher amount of heteroatoms and chemical complexity than lighter fractions. On this macroscopic scale, aging effects are hardly noticeable and are discussed at the molecular level below.

In order to support the findings from TG-FT-ICR MS experiments, GC×GC-HRTOFMS was complementary applied enabling the separation of isomers and a more detailed identification of molecular structures. The application of EI with 70 eV, as universal ionization technique, further enables the detection of nonpolar hydrocarbons, such as alkanes or cycloalkanes. The class distribution of the gas chromatographic data is depicted in Figure 1 (bottom) revealing the predominance of non-polar to semi-polar species. As a chromatographic-based technique, only volatile compounds could be targeted, which excludes high-molecular species in the model bitumen. However, with the applied high-temperature method, species with m/z up to 600 could be detected. The desorption phase observed during TG-FT-ICR MS is to a great extent congruent with the boiling range covered by GC×GC-HRTOFMS allowing to confirm structural assessments derived from elemental compositions as well as the calculated DBE [65]. Due to the compositional continuum of crude oil-derived material [55], structural motives, obtained by GC×GC-HRTOFMS for desorbable species, can be extrapolated to non-volatile compounds observed during the pyrolysis phase with TG-FT-ICR MS.

General alterations

The first information on the aging process can be obtained from the mass loss curves of the TG measurements and its derivative (DTG) in Figure 2 a) and b), respectively. The comparison of the averaged mass loss curves of the non-aged and the 7 days-aged model bitumen reveals a decrease of the mass loss in the desorption phase from 62.5 ± 2.2 % to 56.5 ± 2.1 % during aging and an increase of the pyrolysis phase from 29 ± 0.8 % to 31.3 ± 0.8 %. In addition, the averaged non-evaporable residue increases from 8.5 ± 1.9 % to 12.2 ± 1.4 %, which leads to the assumption that low-boiling

compounds are evaporated or transformed into higher boiling point species during the aging under elevated temperatures. This conjecture is supported by the DTG curves showing a shift of the beginning of the desorption phase of about 50 °C from 100 to 150 °C after 7 days of aging, while the pyrolysis phase starts in both cases at approximately 400 °C. Besides the TG information, also average mass spectrometric data, such as the averaged total ion chromatogram (TIC) depicted in Figure 2 c), reveal a shift to a higher proportion of the pyrolysis phase. In the non-aged model bitumen, 83.0 ± 0.7 % of the TIC account for the desorption phase and 17.0 ± 0.7 % for the pyrolysis phase. After 7 days of aging, the desorption phase is reduced to 81.0 ± 0.5 %, while the pyrolysis phase is increased to 19.0 ± 0.5 %. Further, GC×GC-HRTOFMS data gave evidence, that this shift is partially caused by evaporation due to a decrease for low-boiling semi-volatiles after intensive aging, which is more specifically discussed for the CH-class later. A detailed magnification of the affected region for different aging stages is given in Figure S4, showing that the evaporation effect is most severe after 7 days of aging. Generally, the loss of volatiles is known as an aging effect from literature, causing hardening and embrittlement due to the compositional changes of the bituminous material. Lerfald (2000) stated, that molecular alterations in the presence of air can occur because of the evaporation of existing molecules or the reaction of oxygen with bitumen compounds leading to less volatile species [14]. This effect is most severe at high temperatures or when the material is present in thin films, which is both characteristic for the short term aging during the mixing process of bitumen and aggregates [2,14].

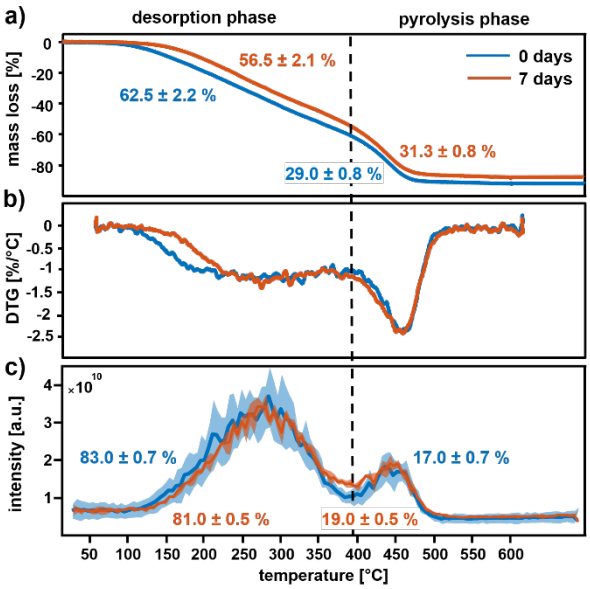

Figure 2: Depiction of the desorption and pyrolysis phase of the model bitumen obtained by TG-APCI-FT-ICR MS. The desorption and pyrolysis phases were separated manually for each spectrum at the dashed line. a) Comparison of the TG curves (3 replicates averaged) of non-aged (blue) and 7 days-aged (orange) model bitumen. Aging shows a shift of the beginning of the desorption phase of about 50 °C up to higher temperatures. Additionally, the non-evaporable residue increases from 10 to 16 %. b) The DTG curves clarify the different starting of the desorption phase of non-aged and 7 days-aged model bitumen. c) Temperature profile of the total ion count (TIC) of non-aged and 7 days-aged model bitumen. The shaded area accounts for the average of three replicates plus/minus the standard deviation.

CH-class and oxidized O_x-classes

The CH-class is the most prevalent chemical class in the model bitumen as revealed by GC×GC-HRTOFMS data. 80-82 % of the classified peak area accounts for hydrocarbons, which can be subdivided into 32-33 % n- and iso-alkanes, 22-24 % cycloalkanes, and 25-26 % aromatics, respectively. Figure 1 illustrates the compound class distribution for 7 days-aged model bitumen for both measurement techniques. The corresponding diagrams for the non-aged sample are given in Figure S5. The FT-ICR MS data show a noticeably lower proportion of the CH-class, which is accounted for by the applied ionization method APCI. Under atmospheric pressure conditions, nonpolar hydrocarbons, such as alkanes and cycloalkanes, cannot be ionized by the chemical ionization process initiated by a corona discharge. Consequently, approximately 55 % of the matrix is disregarded, enabling to focus on heteroatom-containing minorities. Nonetheless, unsaturated CH-species, especially aromatic compounds, are considered by APCI as well. 35-38 % of the intact species in the

desorption phase account for the CH-class, while 37-40 % amount to thermal fragments in the pyrolysis phase.

Table 1: Effects of aging on the model bitumen: Compilation of different parameters obtained from average MS- and MS/MS-data of the desorption and pyrolysis phase of the FT-ICR MS data itemized in compound classes. The trends in bold are verified by the Weir t-test, while trends in parentheses show consistent, but non-significant trends. The abbreviation (des) accounts for the desorption phase, while (pyr) accounts for the pyrolysis phase.

			CH	O1	O2	S1	S1O1	S1O2	S2	S2O1	N1	N1O1	N1S1	N1S2	N2
number of formulae	(des)	MS	-	(↗)	(↗)	-	(↗)	↗	(↘)	-	**↘**	-	(↘)	-	-
		MS/MS	-	↗	↗	-	-	↗	-	↗	**↘**	↗	(↘)	-	**↘**
	(pyr)	MS	-	↗	(↗)	-	↗	-	(↘)	-	(↘)	-	(↘)	-	-
		MS/MS	-	↗	↗	-	↗	↗	-	(↗)	(↘)	↗	(↘)	-	(↘)
summed intensity	(des)	MS	-	↗	-	-	-	↗	-	-	**↘**	-	(↘)	-	-
		MS/MS	-	↗	↗	-	↗	↗	-	↗	(↘)	(↗)	(↘)	-	-
	(pyr)	MS	-	↗	-	-	↗	-	-	-	-	-	(↘)	-	-
		MS/MS	-	↗	↗	-	↗	↗	-	↗	(↘)	↗	(↘)	-	-
intensity-weighed m/z	(des)	MS	-	(↗)	↗	-	-	-	**↘**	-	(↘)	-	(↘)	-	-
		MS/MS	-	↗	(↗)	-	(↗)	(↘)	-	-	-	↗	**↘**	-	(↘)
	(pyr)	MS	(↘)	(↗)	↗	(↘)	-	-	**↘**	-	(↘)	-	**↘**	-	-
		MS/MS	-	↗	-	-	(↗)	-	-	-	(↘)	↗	(↘)	(↘)	(↘)
intensity-weighed DBE	(des)	MS	(↘)	(↗)	↗	-	(↗)	**↘**	↗	-	(↘)	-	(↘)	(↘)	-
		MS/MS	(↘)	-	(↗)	-	↗	**↘**	-	-	(↘)	↗	(↘)	-	-
	(pyr)	MS	(↘)	(↗)	-	-	(↗)	-	-	-	(↘)	-	(↘)	-	-
		MS/MS	-	(↗)	-	-	-	-	-	-	(↘)	-	-	-	-

↗ significant increasing trend during aging
(↗) non-significant increasing trend during aging
↘ significant decreasing trend during aging
(↘) non-significant decreasing trend during aging

For FT-ICR MS data, different average parameters, such as the number of assigned sum formulae, summed intensity, intensity weighed m/z as well as DBE, are investigated concerning the complete aging row of six samples. General trends are summarized in Table 1 and exemplarily depicted as bar graphs for the intact species of the desorption phase in Figure 3. Corresponding information on the pyrolysis phase and MS/MS-spectra are given in Figure S6. The CH-class of the model bitumen shows no significant changes during aging. Nonetheless, while intensity and number of assigned sum formulae stay consistent over the aging time, a slight decrease of the intensity-weighed mean DBE between 0.2 and 0.4 units is observed for the desorption phase and for thermal fragments in the pyrolysis phase. When previously divided into compound classes, DBE vs. carbon number (#C) plots

give an ideal opportunity to investigate the aging process on the molecular level, because the chemical space is spanned by aromaticity (DBE) versus alkylation/molecular size (#C) and additionally, data points can be color-coded with signal intensity. Figure 4 and Figure 5 show the DBE vs. #C plots of selected compound classes for desorption and pyrolysis phase, respectively. In both figures, the aging extrema (0 days vs. 7 days) are compared to underline the aging-related changes. Regions, in which aging effects occurred, are marked to facilitate the discussion. In accordance with the average parameters, the CH-class reveals no changes for the desorption phase in DBE vs. #C diagrams as well. Therefore, evaporation effects can be excluded from FT-ICR MS data and molecular alterations can be attributed to chemical aging effects. GC×GC-HRTOFMS data was used for group type analysis [63,66] of the chemical space. The relative abundance for the dominant 20 functionalities are shown in Figure 6 a), which account together for 96 % of the classified peak area. Information on nonpolar hydrocarbons as well as distinct chemical structures are added to the sum formula attribution of FT-ICR MS data. The averaged abundance of the alkanes, naphthenes, hopanes, benzenes, fluorenes and 3-ring aromatics show no significant alterations over the aging time. However, slight evaporation effects are observed for small hydrocarbons, especially after 7 days of aging. C13- to C16-n-alkanes are prevalently affected. Beyond that, after extensive aging, a slight decrease of the averaged signal intensity is observed for benzonaphthenes, naphthalenes, and biphenyls, which is attributable to evaporation of low boiling homologues. A slight decrease of pyrenes was observed for GC×GC-HRTOFMS data as well, but could not be confirmed by a decrease of DBE 12 for the CH-class in FT-ICR MS data. Nonetheless, the reduction of condensed aromatic species during aging was observed in previous studies by Handle et al. (2017) with ESI-FT-ICR MS [33]. Generally, for both measurement techniques, desorbable CH-species show extremely low alterations, which is congruent for observations of the saturates fraction in classical SARA fractionation, considered as relatively inert against aging in literature [1,14,18,25].

In contrast to intact evaporable species, the pyrolysis phase obtained by TG-FT-ICR MS reveals aging-related changes for high molecular weight CH-compounds. As discernable in Figure 5 a) for 7 days-

aged model bitumen, there is an increase for smaller thermal fragments with carbon numbers between 13 to 29 and DBEs of 4 to 12, corresponding to aromatics with low alkylation. Exemplarily, the species can be tentatively attributed to alkylated benzenes (DBE 4), tetrahydronaphthalenes (DBE 5), naphthalenes (DBE 7), fluorenes (DBE 9), anthracenes/phenanthrenes (DBE 10) or pyrenes/fluoranthenes (DBE 12). The increased detection of these low alkylated aromatics could be explained as follows. The oxidation of hydrocarbons increases their polarity, which subsequently decreases their vapor pressure shifting species from the desorption phase into the pyrolysis phase. Because of the high temperatures during pyrolysis, side chains can be cleaved off. If these chains were oxidized before, the remaining, mostly dealkylated aromatic core is detected as pure CH-compound in the pyrolysis phase. In MS/MS-mode in Figure 5 b), a significant increase for aromatic cores with 14 to 31 carbons is observed, where species with DBE 13 (potentially chrysenes) and DBE 16 (potentially benzochrysenes or other aromatic isomers) are most prevalent. An increase in aromaticity and a decrease of the long-chain index is also known from other studies about bitumen aging [9,24]. Since alterations are mainly found in the pyrolysis phase, it can be assumed that the thermal treatment of the model bitumen affects primarily high molecular-weight CH-species or may lead to their formation.

As expected for oxidative aging, the oxygen-containing classes steadily increase over the aging time. For FT-ICR MS data, the number of assigned sum formulae increases for the O1-class for both measurement modes significantly and the signal intensity grows significantly over the aging time for the desorption and pyrolysis phase. Following the same trend, the intensity-weighed mean *m/z* shows a significant increase for the O1-class of about 30 Da in both phases and modes and reaches approximately the same value as the CH-class after 7 days of aging, which is about 375 Da for the MS-mode and 325 Da in MS/MS-mode in both phases, respectively. DBE vs. #C plots reveal an increase in DBE and alkylation for the desorption and pyrolysis phase of the O1-class in both modes. In the desorption phase depicted in Figure 4 c), species with 15 to 21 carbons show a significant increase in aromaticity, with DBE 9 (potentially oxidized biphenyls) and 10 (potentially fluorenones) being most preferred. These structural considerations are in very good accordance with GC×GC-HRTOFMS data,

which shows carbonyl formation, especially on aromatics with an activated carbon atom, such as fluorenes. Chromatographic information exhibit a distinct significant increase for fluorenones and benzofluorenones corresponding to a direct oxidation of the ring. Contrary, furans, as the investigated dibenzofurans and tribenzofurans, show no significant changes indicating that the formation mechanism of cyclic-bound oxygen seems not to be triggered by short-term aging conditions. For desorbable species in FT-ICR MS data, a preference of oxidation on smaller molecules with high DBE was observed. For example, species potentially attributed to fluorenones (DBE 10) show especially for C1-C5 alkylation a distinct increase, with the C3-alkylated being most favored. A corresponding observation was revealed by GC×GC-HRTOFMS data, where C0-, C1- and C2-alkylated fluorenones occur in increasing order with C2-Fluorenone steadily increasing during the complete aging time (Figure S7). For strong alkylated species, FT-ICR MS data show evidence for a less favored oxidation, which could be explained by an increased steric hindrance for oxidation at the aromatic core. Long or strongly branched alkyl chains of larger molecules may protect the aromatic core against oxidation. In MS/MS-mode for the desorption in Figure 4 d) and especially for the pyrolysis phase in Figure 5 d), a substantial increase in oxidized core structures of high-molecular compounds is observed. This finding is congruent with previous studies in literature, which reported an increase in the resin and asphaltene SARA fractions analyzed with different analytic techniques [1,3,4,25,30,31,33]. The core structures of the pyrolysis fragments observed in this study are most likely formed by species typically attributed to the resin or asphaltene fraction. Although the O2-class shows no significant changes for MS-mode in the FT-ICR MS data, the core structures occurring in the desorption and pyrolysis phase in MS/MS-mode reveal the same trends in signal intensity and a number of formulae as exhibited by the O1-class. In addition, DBE vs. #C plots show an increase for O2-species with a comparatively high DBE between 10 and 18 for the desorption phase and 12 and 20 for the pyrolysis phase. As a consequence, multiple oxidations seem to take place favorably at high aromatic structures. The fact that various oxidized compounds survive the fragmentation during the CID process leads to the assumption, that oxidation takes place at the aromatic core or at a position close to the aromatic ring forming, most

likely, a ketone [1,13]. This hypothesis is supported by Petersen et al. (1998) and Dorrence et al. (1974) who found strong evidence that carbonyls are preferentially formed at the carbon in benzylic position [26–28].

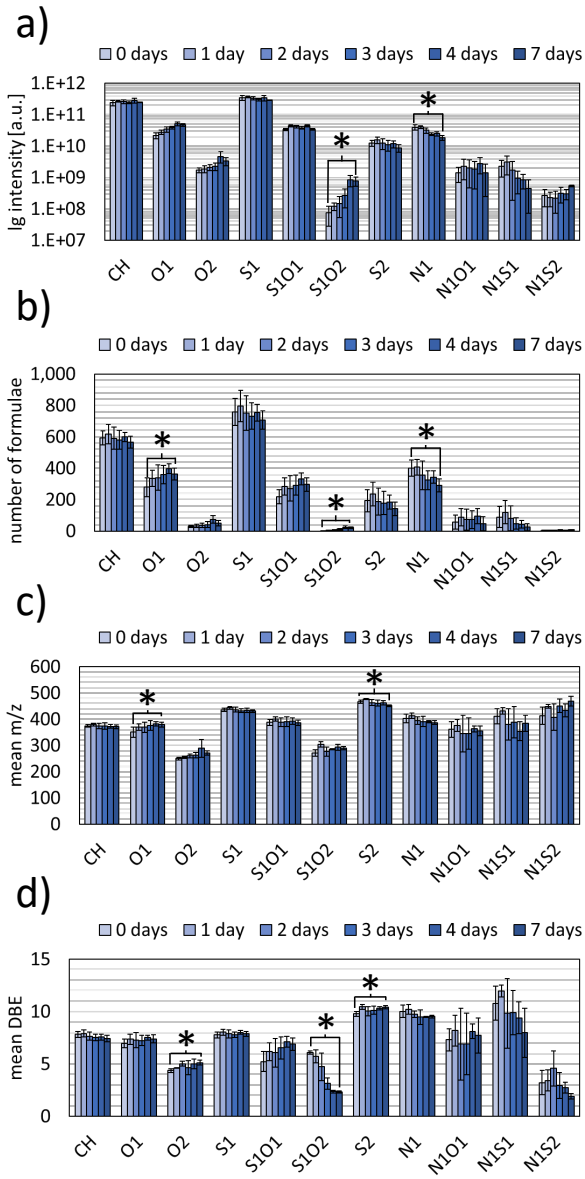

Figure 3: Overview of considered average parameters exemplarily depicted for the desorption phase in normal MS-mode for the model bitumen over the aging time. The shown compound classes account for over 99 % of the assigned signal TIC. a) The log(10) summed intensity for easier investigation of the aging trends of low abundant compound classes, b) the number of calculated formulae, c) the mean intensity-weighed m/z, d) the mean intensity-weighed DBE. The asterisks mark significant differences with a statistical reliability of 95 % between the parameters in the non-aged sample and the 7 days-aged model bitumen.

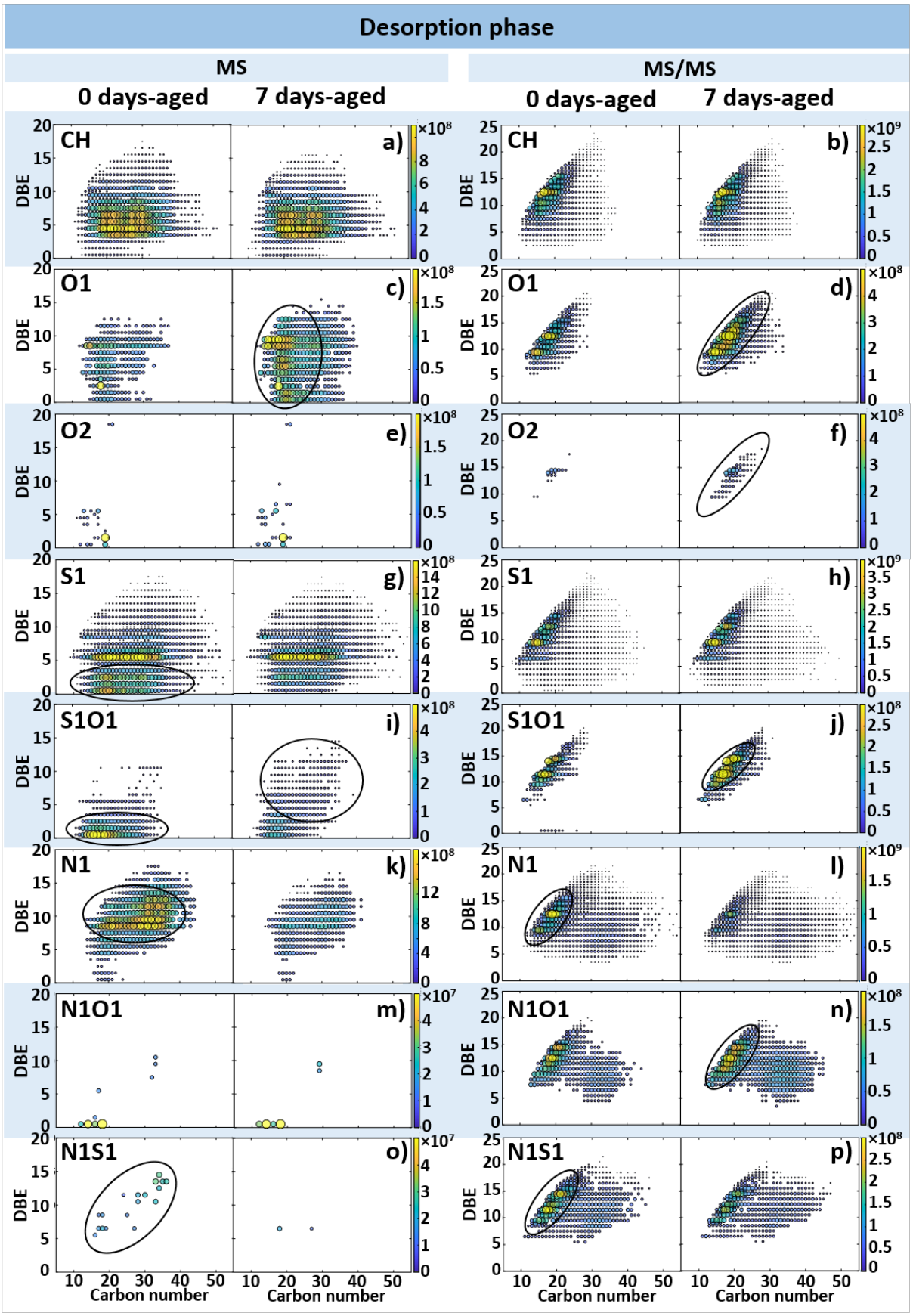

Figure 4: Double bond equivalent (DBE) versus the number of carbon atoms (#C) plots of different compound classes obtained from the desorption phase of the TG-FT-ICR MS data in MS- and MS/MS-mode for non-aged and 7 days-aged model bitumen. The size and color of the data points correlate with the signal intensity. The shown species were found in all three replicates.

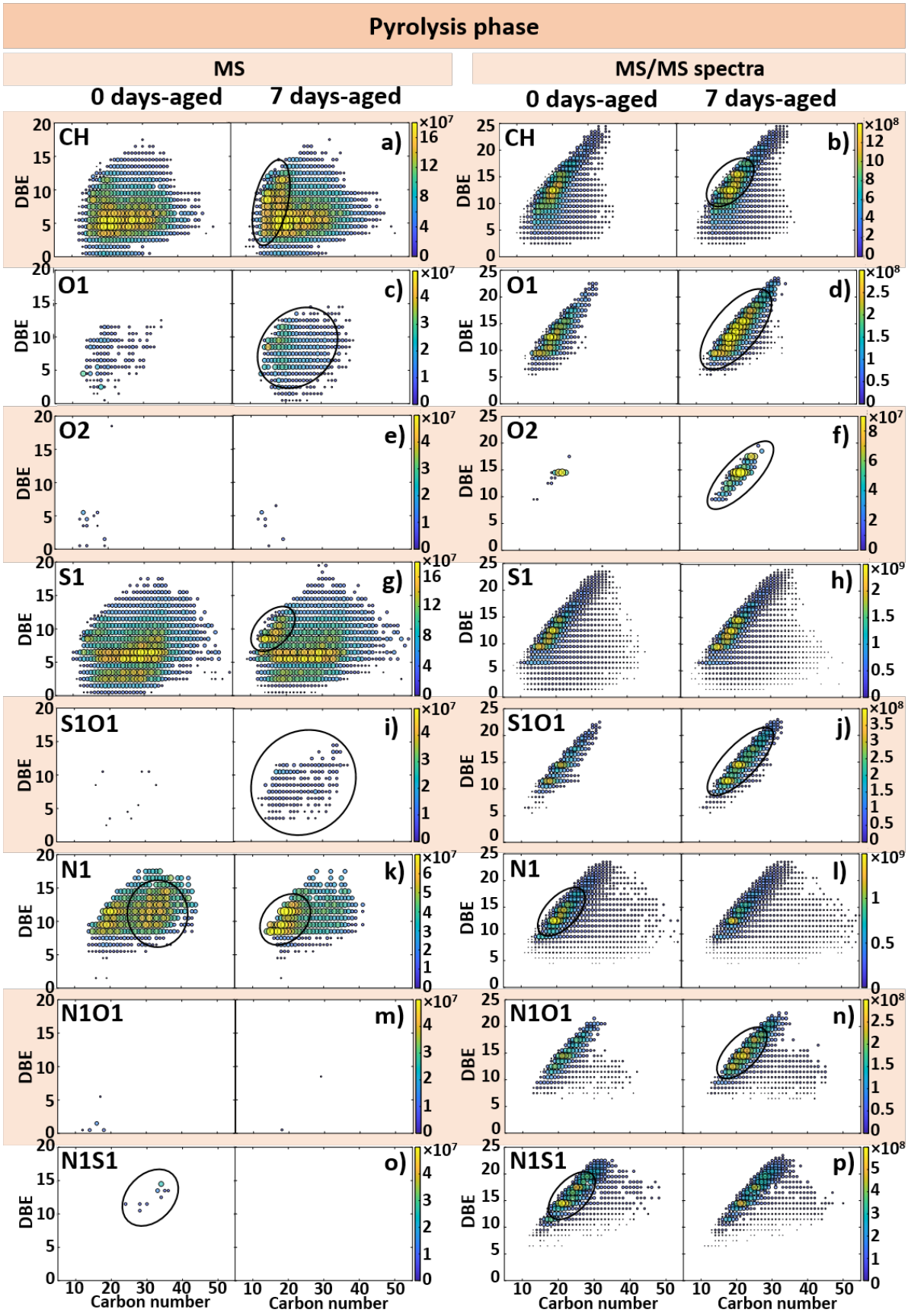

Figure 5: Double bond equivalent (DBE) versus the number of carbon atoms (#C) plots of different compound classes obtained from the pyrolysis phase of the TG-FT-ICR MS data in MS- and MS/MS-mode for non-aged and 7 days-aged model bitumen. The size and color of the data points correlate with the signal intensity. The shown species were found in all three replicates.

S_x-classes and oxidized S_xO_y-classes

For FT-ICR MS data, the S1-class is the compound class with the highest signal intensity and a number of assigned sum formulae with a mean *m/z* of 430 for MS-mode and 390 to 400 for MS/MS-mode as well as a mean DBE of 7.9 to 8.6 and 10.3 to 11.5, respectively. The discrepancy to the GC×GC-HRTOFMS data, where hydrocarbons are prevalently represented, is explicable by the application of APCI highlighting more polar compounds. The average parameters of the S1-class obtained with FT-ICR MS show no significant changes in average parameters over the aging time. Nonetheless, the comparison of the DBE vs. #C plots of the desorption phase in Figure 4 g) reveals that compounds with DBE < 4 decrease significantly. These species may involve the tetrahydrothiophenes (DBE 1) measured with GC×GC-HRTOFMS, which show a significant decrease as depicted in Figure 6 a) and c). In contrast, higher DBE compounds, such as benzothiophenes (DBE 6), dibenzothiophenes (DBE 9), and benzonaphthothiophenes (DBE 12) show no changes during aging in GC×GC-HRTOFMS data. The same observation was made with FT-ICR MS, where the predominant intact species with DBE 6, which can tentatively be attributed to benzothiophenes, and the major core structures with DBE 10, 12 and 13 (potentially benzylbenzothiophenes, benzonaphthothiophenes, benzonaphtho-thiophenes with an attached saturated ring) [67–69] reveal hardly any alterations. Regarding the pyrolysis phase in MS-mode in Figure 5 g), a slight decrease in intensity for low DBE S1-compounds is observed as well. However, for species with DBE 9 to 12 and carbon numbers between 10 and 20, an increase in signal intensity is revealed. This observation can be explained by the formation of oxidation products at the side chains of the molecules, which are cleaved off during pyrolysis leading to the detection of the non-oxidized thermal fragment. This reaction is discussed in detail for the CH-class above. Besides the S1-class, the S2-class and for MS/MS-spectra also the S3-class were observed with low abundancies. The classes with more than one sulfur atom have, in general, a higher mean *m/z* and mean DBE, which is typically observed for petroleum-derived material [70,71]. Only minor alterations are caused by aging for the classes containing two to three sulfur atoms. A significant decrease of the intensity-weighed mean *m/z* is observed for the S2-class in MS-mode, indicating a reduction in alkylation. In general, our results

exhibit that non-aromatic sulfur components show a higher reactivity to oxidative aging than aromatic sulfur species. Lobodin et al. (2015) already revealed that crude oil is composed of reactive (sulfides, disulfides, and thiols) and non-reactive (thiophenes and diaryl sulfides) sulfur species [68]. Furthermore, Porto et al. (2019) found evidence, that asphalt concretes containing a high amount of non-aromatic sulfur compounds are prevalently affected by short-term aging [72].

According to previous studies [1,9,26,28], sulfoxides are one of the main functional groups formed during oxidative aging in bitumen. For FT-ICR MS data, already the average parameters for core structures in the desorption phase and for both modes in the pyrolysis phase reveal a distinct increase of the S1O1-class. At first glance, however, the average intensity as well as the number of assigned sum formulae stay consistent over the aging time for intact species in the desorption phase. Nevertheless, the in-depth investigation at the molecular level in Figure 4 i) reveals alterations during aging as well. In the non-aged model bitumen, S1O1-species with DBE 1 to 2 are prevalent, while these species are significantly reduced after 7 days of aging and higher DBE species occur. Figure S8 illustrates the DBE vs. #C diagrams opposing for the O1-class and the S1O1-class for the whole aging row. While the O1-class shows a distinct increase in smaller molecules as described above, the S1O1-class shows after 1 day of aging an increase in species with a low DBE of 1 to 2. With proceeding aging time, the low DBE species decrease significantly, whereas higher DBE compounds are formed. By investigation of the DBE vs. #C diagram of the S1O2-class of the desorption phase in MS-mode, we found evidence that the reduction of the low DBE compounds in S1O1-class correlates with an increase in low DBE species in the S1O2-class (Figure S9). Due to very low intensity, the S2O1-class was only detected for the complete aging row in MS/MS-mode but follows the same trend as other oxidized sulfur-containing classes. The core structures showed a significant increase in the average number of sum formulae as well as the average signal intensity. In Figure S10 a), the DBE vs. #C diagram of the desorption phase reveals a distinct increase in the intensity of S2O1-core structures with DBEs between 12 and 17. For desorbable oxidized sulfur-containing compounds, only a few additional structural information could be obtained with GC×GC–HRTOF MS due to the nominal proportion of this kind of components.

Nonetheless, for dibenzothiophene-oxides, an increase in signal intensity was observed over the aging time as depicted in Figure 6 d).

Regarding the pyrolyzed compounds of the FT-ICR MS data in Figure 5 i), only very few S1O1-species could be found in the non-aged model bitumen, but the number and signal intensity increased significantly after 7 days of aging. The MS/MS-mode reveals an increase in signal intensity for high aromatic core structures of intact S1O1-species and their pyrolysis fragments. In the desorption phase, prevalently compounds with a DBE of 10 to 15 increase, while in the pyrolysis phase species with DBE 12, DBE 15, and DBE 18 are mostly favored. The latter can be tentatively attributed to oxidized benzonaphthothiophenes and further attached fused aromatic rings. Besides the S1O1-class, the S2O1-class shows a significant increase for average intensity in MS/MS-mode as well. At the molecular level, the signal intensity raises predominantly for species between DBE 12 and 20 in the pyrolysis phase, as depicted in Figure S10 b).

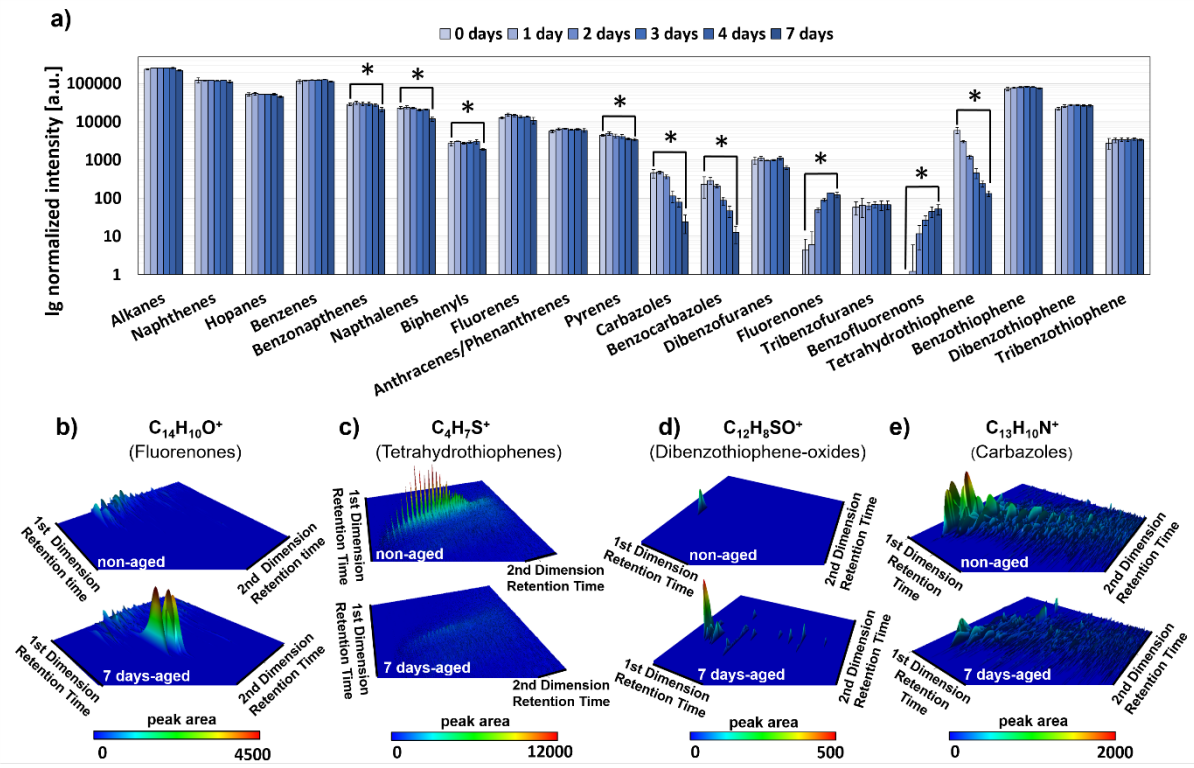

Figure 6: Compilation of GC×GC-HRTOFMS data of different aging effects on selected compound classes investigated in the model bitumen. a) Investigated compound classes in non-aged to 7 days-aged model bitumen after group-type analysis. The 20 depicted compound classes account for 96 % of the classified peak area. Significant changes between non-aged and 7 day-aged bitumen are marked with an asterisk. The significance with 95 % statistic certainty was investigated with the Weir t-test.

b) Survey view of the $C_{14}H_{10}O^+$-fragment corresponding to fluorenones. After 7 days of aging, the signal intensity of the fragment is clearly increased. c) Survey view of the $C_4H_7S^+$-fragment corresponding to tetrahydrothiophenes. Aging clearly reduces the signal intensity of the fragment. d) Survey view of the $C_{12}H_8SO^+$-fragment corresponding to Dibenzothiophene-oxides. Aging increases the signal intensity of the fragment, but it remains near the detection level. e) Survey view of the $C_{13}H_{10}N^+$-fragment corresponding to carbazoles. After 7 days of aging, the signal intensity of the fragment is clearly reduced.

N_X-class, NS-class and oxidized NO-classes

Although oxides and sulfoxides are often investigated with respect to bitumen aging in literature, nitrogen-containing species are rarely considered. To the best of the authors' knowledge, solely Handle et al. (2017) report an increase of oxidized NO_{1-9}-compounds in long-term aged bitumen investigated with direct infusion ESI-FT-ICR MS [33]. Compatible to these results, a substantial loss of volatile N1-compounds was observed for the model bitumen in this study. The average parameters revealed by FT-ICR MS measurements exhibited a significant reduction in the number of molecular formulae and signal intensity of the N1-class during the desorption phase. Due to the very low abundance, the N2-class could only be detected in MS/MS-mode, but shows the same significant decrease as the N1-class. Regarding the DBE vs. #C plots in Figure 4 k), non-aged bitumen shows a comparable high intensity for intact N1-species with a DBE of 9-13, which can tentatively be attributed to benzoindoles or carbazoles (DBE 9), acridines (DBE 10), tetrahydroacridines or benzylacridines (DBE 11), indenoquinolines or benzocarbazoles (DBE 12) as well as benzacridines (DBE 13) [69,73,74]. After 7 days of aging, the previously mentioned molecular structures are severely reduced. A similar observation was made for the MS/MS-mode of the desorption phase in Figure 4 l), where a strong reduction of the dominant DBE lines of 10 and 13, potentially attributed to acridines and benzacridines, is observed. In addition, GC×GC-HRTOFMS measurements reveal a strong and distinct decrease in intact carbazolic and benzocarbazolic structures as well, partially validating the proposed structures from FT-ICR MS. The decrease for the $C_{13}H_{10}N_1^+$, which is a typical electron ionization fragment ion of carbazoles, is highlighted in Figure 6 e). However, no evidence for acridinic structures was found in the GC×GC-HRTOFMS data. Concerning the pyrolysis phase in Figure 5 k) and l), high-molecular thermal fragments, such as species with a DBE between 9 to 15 and carbon numbers

between 26 to 38, show a distinct decrease after 7 days of aging. The same trend is observed for aromatic core structures in MS/MS-mode as well, where compounds with a DBE of 13 (possibly benzacridines) to DBE of 15 (possibly phenanthrocarbazoles) are prevalently reduced. However, different from the predominantly observed decrease of the N1-class, small molecular pyrolysis fragments, especially with DBE 9 (possibly carbazoles), DBE 10 (possibly acridines), and DBE 12 (possibly benzocarbazoles), are increased during aging in the MS-mode. A possibility for the observed increase is discussed in the following. The most apparent hypothesis explaining the general decrease of the N1-class is a strong oxidation of the N1-containing compounds. However, the DBE vs. #C plots for the MS-mode show no increase of the intact species or pyrolysis fragments of the N1O1-class. Furthermore, with GC×GC-HRTOFMS, no oxidized nitrogen-containing compounds could be detected. The absence of newly formed N1O1-compounds in MS-mode and chromatographic measurements can be explained by the poor signal intensity of the oxidized products remaining below the detection limit. Another explanation is the decrease of the N1-class due to intermolecular reactions triggered by the high aging temperatures of about 150 to 160 °C. High reaction temperatures can lead, for example, to the condensation of indole-derivatives on acridine-like structures obtained in high yields in literature [75]. The condensates have a higher molecular weight and, therefore, a higher vapor pressure, converting previously evaporable species into compounds occurring in the pyrolysis phase. Evidence for this hypothesis can be abstracted from the 7 days-aged N1-class in Figure 5 k). In MS-mode, smaller pyrolysis fragments with carbon numbers of 15 to 25 reveal an increase in signal intensity, indicating cracking of newly formed N-containing condensates. Besides the N1-class, N2-class core structures reveal a similar decrease in signal intensity for the desorption and pyrolysis phase, which is shown in Figure S10 a) and b). Due to the low concentration of these species, the N2-class is hardly detectable after 7 days of aging.

Although the MS-mode reveals no increase in oxidized nitrogen-containing components, a preferred oxidation of high aromatic core structures is indicated by MS/MS-spectra due to a distinct increase in the number of assigned sum formulae, signal intensity, mean *m/z* and mean DBE for the N1O1-class.

With respect to Figure 4 n) and Figure 5 n), core structures with a DBE of 10-16 reveal a clear increase in intensity for N1O1-compounds in the desorption phase, while the oxidation is also pronounced for species with a DBE up to 20 in the pyrolysis phase.

In addition to pure N-containing classes, the N1S1-class show a slight decrease in average signal intensity, a number of sum formulae, mean *m/z*, and DBE as well. Equally to other classes containing more than one heteroatom, the N1S1-species show a comparable high mean DBE and are mostly detected in the MS/MS-spectra as high aromatic core structures, which is explicable by the Boduszynski model. The model predicts the occurrence of N- and S-atoms in one molecule only for bigger aromatic structures in crude oil-derived material and was proven by several FT-ICR MS studies. [52–54] With respect to the studied aging effects in the desorption phase in Figure 4 p), the N1S1-class shows mainly a reduction of the DBE lines of 12, 13 and 15 of the core structures, which can tentatively be attributed to benzothienoquinolines, benzylthienoquinolines, and dibenzothienoquinolines, respectively [69]. In the pyrolysis phase, species with DBEs of 12, 15, and 18 are primarily reduced. The few species detected for MS-mode disappeared nearly completely after 7 days of aging.

Conclusion

The combination of TG-APCI-FT-ICR MS and GC×GC-HRTOFMS revealed complementary and consistent results on different chemical changes occurring during prolonged short-term aging in a specially generated model bitumen. Polar to semi-polar as well as semi-volatile to pyrolyzable species were highlighted at the molecular level by TG-APCI-FT-ICR MS. Supporting GC×GC-HRTOFMS enabled the validation of FT-ICR MS data for semi-volatile compounds and contribute insights on aging processes on selected molecular structures and distinct functionalities. The main changes attributed to aging can be summarized as follows:

- The CH-class is relatively inert against aging, nonetheless, pyrolysis fragments and their corresponding core structures show a shift to smaller carbon numbers with less alkylation.
- The O1-class and especially fluorenones increase significantly in signal intensity. Smaller molecules of the O1-class are preferred oxidized, while the O2-class occurs primarily for high molecular-weight structures.
- The S1-class significantly decreases for non-aromatic species (especially tetrahydrothiophenes), while aromatic sulphur components, such as thiophenic structures, reveal no changes. Pyrolysis fragments increase for species with lower carbon numbers with comparatively high DBE, which might be attributed to dealkylation during aging. For the S1O1-class, low-DBE compounds decrease probably due to further oxidation, while high-DBE species are formed.
- One of the strongest observed effects was the depletion of nitrogen-containing structures, especially for carbazolic structures. An increase in intact oxidized N-species that evolve in the desorption phase could not be detected. Nonetheless, an increase of small N-species with comparatively high DBE are formed during aging in the pyrolysis phase, potentially caused by thermally-induced condensation reactions due to high aging temperatures. For core structures, an increase of N1O1-species was observed.

To conclude, the macroscopic changes observed in the physical properties of bitumen may derive from the formation of polar components such as O-, SO- and NO-containing species, which are primarily observed for high aromatic compounds as well as the reduction of species with low aromaticity and N-containing species in general. Further, the combination of both techniques can be beneficial for the analysis of a variety of analytically challenging complex mixtures, which essentially need a multi-method approach for a detailed chemical description.

The deep understanding of bitumen aging will help to improve the quality of bitumen binders and could increase the durability of the pavement. Future studies on bitumen aging will focus on how

different laboratory aging methods as well as more realistic aging[76], further treatment or the addition of additives affect the chemical composition of the aged material.

Acknowledgements

Funding by the Horizon 2020 program for the EU FT-ICR MS project (European Network of Fourier-Transform Ion-Cyclotron-Resonance Mass Spectrometry Centers, Grant agreement ID: 731077) is gratefully acknowledged. The authors thank the German Research Foundation (DFG) for funding of the Bruker FT-ICR MS (INST 264/56). Financial support by ZIM (Zentrales Innovationsprogramm Mittelstand, Germany, grant ID: ZF4198001SL6) is gratefully acknowledged.

Supporting information

- Additional information on measurement parameters of FT-ICR MS (Table S1) and GC×GC-HRTOF MS (Table S2)
- Data quality proof for FT-ICR MS measurements (Figure S1)
- Additional time-resolved FT-ICR MS spectra for non-aged and 7days-aged model bitumen (Figure S2)
- GC×GC-HRTOF MS chromatograms for non-aged and 7days-aged model bitumen (Figure S3) as well as details showing evaporation for low-boiling components after severe aging (Figure S4)
- Compound class distribution for non-aged model bitumen for both techniques (Figure S5)
- Average parameters obtained by FT-ICR MS measurements for both modes and phases as well as all examined classes (Figure S6)

- Aging effect of fluorenones with different alkylation degree revealed by GC×GC-HRTOFMS (Figure S7)
- Additional DBE vs. #C diagrams of FT-ICR MS data for O1-, S1O1-, S1O2-, S2O1- and N2-class (Figure S8, S9 and S10)

References

(1) Petersen, J. C. *A Review of the Fundamentals of Asphalt Oxidation: Chemical, Physicochemical, Physical Property, and Durability Relationships*; Transportation Research Board: Washington, D.C., 2009.

(2) Lesueur, D. The colloidal structure of bitumen: consequences on the rheology and on the mechanisms of bitumen modification. *Adv. Colloid Interface Sci.* 2009, *145*, 42–82.

(3) Rebelo, L. M.; Sousa, J. S. de; Abreu, A. S.; Baroni, M.P.M.A.; Alencar, A.E.V.; Soares, S. A.; Mendes Filho, J.; Soares, J. B. Aging of asphaltic binders investigated with atomic force microscopy. *Fuel* 2014, *117*, 15–25.

(4) Chipps, J. F.; Davison, R. R.; Glover, C. J. A Model for Oxidative Aging of Rubber-Modified Asphalts and Implications to Performance Analysis. *Energy Fuels* 2001, *15*, 637–647.

(5) Themeli, A.; Chailleux, E.; Farcas, F.; Chazallon, C.; Migault, B.; Buisson, N. Molecular structure evolution of asphaltite-modified bitumens during ageing; Comparisons with equivalent petroleum bitumens. *Int. J. Pavement Res. Technol.* 2017, *10*, 75–83.

(6) Branthaver, J. F.; Petersen, J. C.; Robertson, R. E.; Duvall, J. J.; Kim, S. S.; Harnsberger, P. M.; Mill, T.; Ensly, E. K.; Barbour, F. A.; Scharbron, J. F. *Binder Characterization and Evaluation: Volume 2: Chemistry*; Strategic Highway Research Program. National Research Council. National Academy of Sciences, 1993.

(7) Hofko, B.; Hospodka, M. Rolling Thin Film Oven Test and Pressure Aging Vessel Conditioning Parameters: Effect on Viscoelastic Behavior and Binder Performance Grade. *Transp. Res. Rec.* 2016, *2574*, 111–116.

(8) Hofko, B.; Cannone Falchetto, A.; Grenfell, J.; Huber, L.; Lu, X.; Porot, L.; Poulikakos, L. D.; You, Z. Effect of short-term ageing temperature on bitumen properties. *Road Mater. Pavement Des.* 2017, *18*, 108–117.

(9) Tarsi, G.; Varveri, A.; Lantieri, C.; Scarpas, A.; Sangiorgi, C. Effects of Different Aging Methods on Chemical and Rheological Properties of Bitumen. *J. Mater. Civ. Eng.* 2018, *30*, 4018009.

(10) Bonaquist, R.; Anderson, D. A. *Investigation of Short-Term Laboratory Aging of Neat and Modified Asphalt Binders*; National Academies Press: Washington, D.C., 2011.

(11) Bahia, H. U.; Anderson, D. A. The Pressure Aging Vessel (PAV): A Test to Simulate Rheological Changes Due to Field Aging. In *Physical properties of asphalt cement binders*; Hardin, J. C., Ed.; STP / ASTM 1241; ASTM International: Philadelphia, Pa., 1995; 67-67-22.

(12) Elwardany, M. D.; Yousefi Rad, F.; Castorena, C.; Kim, Y. R. Evaluation of asphalt mixture laboratory long-term ageing methods for performance testing and prediction. *Road Mater. Pavement Des.* 2017, *18*, 28–61.

(13) Petersen, J. C. *Binder characterization and evaluation*; Strategic Highway Research Program, National Research Council: Washington, D.C., 1994.

(14) Lerfald, B. O. *Ageing and Degradation of Asphalt Pavements on Low Volume Roads,: P.h.D. Thesis*; Department of Road and Railway Engineering, The Norwegian University of Science and Technology NTNU, 2000.

(15) Noureldin, A. S. Oxidation of Asphalt Binders and its Effect on Molecular Size Distribution and Consistency. In *Physical properties of asphalt cement binders*; Hardin, J. C., Ed.; STP / ASTM 1241; ASTM International: Philadelphia, Pa., 1995; 137-137-17.

(16) Ehinola, O. A.; Falode, O. A.; Jonathan, G. Softening point and Penetration Index of bitumen from parts of Southwestern Nigeria. *NAFTA* 2012, *63*, 319–323.

(17) Grilli, A.; Gnisci, M. I.; Bocci, M. Effect of ageing process on bitumen and rejuvenated bitumen. *Constr. Build. Mater.* 2017, *136*, 474–481.

(18) Eberhardsteiner, L.; Füssl, J.; Hofko, B.; Handle, F.; Hospodka, M.; Blab, R.; Grothe, H. Towards a microstructural model of bitumen ageing behaviour. *Int. J. Pavement Eng.* 2015, *16*, 939–949.

(19) Eberhardsteiner, L.; Füssl, J.; Hofko, B.; Handle, F.; Hospodka, M.; Blab, R.; Grothe, H. Influence of asphaltene content on mechanical bitumen behavior: experimental investigation and micromechanical modeling. *Mater. Struct.* 2015, *48*, 3099–3112.

(20) Hofko, B.; Eberhardsteiner, L.; Füssl, J.; Grothe, H.; Handle, F.; Hospodka, M.; Grossegger, D.; Nahar, S. N.; Schmets, A. J. M.; Scarpas, A. Impact of maltene and asphaltene fraction on mechanical behavior and microstructure of bitumen. *Mater. Struct.* 2016, *49*, 829–841.

(21) Baek, C.; Underwood, B. S.; Kim, Y. R. Effects of Oxidative Aging on Asphalt Mixture Properties. *Transp. Res. Rec.* 2012, *2296*, 77–85.

(22) ASTM D2007-19. *Test Method for Characteristic Groups in Rubber Extender and Processing Oils and Other Petroleum-Derived Oils by the Clay-Gel Absorption Chromatographic Method*; ASTM International: West Conshohocken, PA.

(23) Mikhailenko, P.; Bertron, A.; Ringot, E. Methods for Analyzing the Chemical Mechanisms of Bitumen Aging and Rejuvenation with FTIR Spectrometry. *International Symposium on Testing and Characterization of Sustainable and Innovative Bituminous Materials* 2016, *11*, 203–214.

(24) Nivitha, M. R.; Prasad, E.; Krishnan, J. M. Ageing in modified bitumen using FTIR spectroscopy. *Int. J. Pavement Eng.* 2016, *17*, 565–577.

(25) Le Guern, M.; Chailleux, E.; Farcas, F.; Dreessen, S.; Mabille, I. Physico-chemical analysis of five hard bitumens: Identification of chemical species and molecular organization before and after artificial aging. *Fuel* 2010, *89*, 3330–3339.

(26) Petersen, J. C.; Glaser, R. Asphalt Oxidation Mechanisms and the Role of Oxidation Products on Age Hardening Revisited. *Road Mater. Pavement Des.* 2011, *12*, 795–819.

(27) Dorrence, S. M.; Barbour, F. A.; Petersen, J. C. Direct evidence of ketones in oxidized asphalts. *Anal. Chem.* 1974, *46*, 2242–2244.

(28) Petersen, J. C. A dual, sequential mechanism for the oxidation of petroleum asphalts. *Pet. Sci. Technol.* 1998, *16*, 1023–1059.

(29) Corbett, L. W. Composition of asphalt based on generic fractionation, using solvent deasphaltening, elution-adsorption chromatography, and densimetric characterization. *Anal. Chem.* 1969, *41*, 576–579.

(30) Allen, R. G.; Little, D. N.; Bhasin, A. Structural Characterization of Micromechanical Properties in Asphalt Using Atomic Force Microscopy. *J. Mater. Civ. Eng.* 2012, *24*, 1317–1327.

(31) Gamarra, A.; Ossa, E. A. Thermo-oxidative aging of bitumen. *Int. J. Pavement Eng.* 2016, *19*, 641–650.

(32) Weigel, S.; Stephan, D. Modelling of rheological and ageing properties of bitumen based on its chemical structure. *Mater. Struct.* 2017, *50*, 83.

(33) Handle, F.; Harir, M.; Füssl, J.; Koyun, A. N.; Grossegger, D.; Hertkorn, N.; Eberhardsteiner, L.; Hofko, B.; Hospodka, M.; Blab, R.*; et al.* Tracking Aging of Bitumen and Its Saturate, Aromatic, Resin, and Asphaltene Fractions Using High-Field Fourier Transform Ion Cyclotron Resonance Mass Spectrometry. *Energy Fuels* 2017, *31*, 4771–4779.

(34) Le Maître, J.; Hubert-Roux, M.; Paupy, B.; Marceau, S.; Rüger, C. P.; Afonso, C.; Giusti, P. Structural analysis of heavy oil fractions after hydrodenitrogenation by high-resolution tandem mass spectrometry and ion mobility spectrometry. *Faraday Discuss.* 2019, *218*, 417–430.

(35) Smith, D. F.; Rodgers, R. P.; Rahimi, P.; Teclemariam, A.; Marshall, A. G. Effect of Thermal Treatment on Acidic Organic Species from Athabasca Bitumen Heavy Vacuum Gas Oil, Analyzed by Negative-Ion Electrospray Fourier Transform Ion Cyclotron Resonance (FT-ICR) Mass Spectrometry. *Energy Fuels* 2009, *23*, 314–319.

(36) McKenna, A. M.; Marshall, A. G.; Rodgers, R. P. Heavy Petroleum Composition. 4. Asphaltene Compositional Space. *Energy Fuels* 2013, *27*, 1257–1267.

(37) Podgorski, D. C.; Corilo, Y. E.; Nyadong, L.; Lobodin, V. V.; Bythell, B. J.; Robbins, W. K.; McKenna, A. M.; Marshall, A. G.; Rodgers, R. P. Heavy Petroleum Composition. 5. Compositional and Structural Continuum of Petroleum Revealed. *Energy Fuels* 2013, *27*, 1268–1276.

(38) Rodgers, R. P.; McKenna, A. M. Petroleum analysis. *Anal. Chem.* 2011, *83*, 4665–4687.

(39) Hourani, N.; Andersson, J. T.; Möller, I.; Amad, M.'a.; Witt, M.; Sarathy, S. M. Atmospheric pressure chemical ionization Fourier transform ion cyclotron resonance mass spectrometry for complex thiophenic mixture analysis. *Rapid Commun. Mass Spectrom.* 2013, *27*, 2432–2438.

(40) Rüger, C. P.; Grimmer, C.; Sklorz, M.; Neumann, A.; Streibel, T.; Zimmermann, R. Combination of Different Thermal Analysis Methods Coupled to Mass Spectrometry for the Analysis of Asphaltenes and Their Parent Crude Oils: Comprehensive Characterization of the Molecular Pyrolysis Pattern. *Energy Fuels* 2018, *32*, 2699–2711.

(41) Rüger, C. P.; Neumann, A.; Sklorz, M.; Schwemer, T.; Zimmermann, R. Thermal Analysis Coupled to Ultrahigh Resolution Mass Spectrometry with Collision Induced Dissociation for Complex Petroleum Samples: Heavy Oil Composition and Asphaltene Precipitation Effects. *Energy Fuels* 2017, *31*, 13144–13158.

(42) Jennerwein, M. K.; Sutherland, A. C.; Eschner, M.; Gröger, T.; Wilharm, T.; Zimmermann, R. Quantitative analysis of modern fuels derived from middle distillates – The impact of diverse compositions on standard methods evaluated by an offline hyphenation of HPLC-refractive index detection with GC×GC-TOFMS. *Fuel* 2017, *187*, 16–25.

(43) Jennerwein, M. K.; Eschner, M. S.; Wilharm, T.; Zimmermann, R.; Gröger, T. M. Proof of Concept of High-Temperature Comprehensive Two-Dimensional Gas Chromatography Time-of-Flight Mass Spectrometry for Two-Dimensional Simulated Distillation of Crude Oils. *Energy Fuels* 2017, *31*, 11651–11659.

(44) Dutriez, T.; Courtiade, M.; Thiébaut, D.; Dulot, H.; Hennion, M.-C. Improved hydrocarbons analysis of heavy petroleum fractions by high temperature comprehensive two-dimensional gas chromatography. *Fuel* 2010, *89*, 2338–2345.

(45) Pollo, B. J.; Alexandrino, G. L.; Augusto, F.; Hantao, L. W. The impact of comprehensive two-dimensional gas chromatography on oil & gas analysis: Recent advances and applications in petroleum industry. *Trends Anal. Chem.* 2018, *105*, 202–217.

(46) Vanini, G.; Pereira, V. B.; Romão, W.; Gomes, A. O.; Oliveira, L. M. S.L.; Dias, J. C. M.; Azevedo, D. A. Analytical advanced techniques in the molecular-level characterization of Brazilian crude oils. *Microchem. J.* 2018, *137*, 111–118.

(47) Ávila, B. M. F.; Vaz, B. G.; Pereira, R.; Gomes, A. O.; Pereira, R. C. L.; Corilo, Y. E.; Simas, R. C.; Nascimento, H. D. L.; Eberlin, M. N.; Azevedo, D. A. Comprehensive Chemical Composition of Gas Oil Cuts Using Two-Dimensional Gas Chromatography with Time-of-Flight Mass Spectrometry and Electrospray Ionization Coupled to Fourier Transform Ion Cyclotron Resonance Mass Spectrometry. *Energy Fuels* 2012, *26*, 5069–5079.

(48) Tessarolo, N. S.; Silva, R. C.; Vanini, G.; Pinho, A.; Romão, W.; Castro, E. V.R. de; Azevedo, D. A. Assessing the chemical composition of bio-oils using FT-ICR mass spectrometry and comprehensive two-dimensional gas chromatography with time-of-flight mass spectrometry. *Microchem. J.* 2014, *117*, 68–76.

(49) Tessarolo, N. S.; Silva, R. V.S.; Vanini, G.; Casilli, A.; Ximenes, V. L.; Mendes, F. L.; Rezende Pinho, A. de; Romão, W.; Castro, E. V.R. de; Kaiser, C. R.*; et al.* Characterization of thermal and catalytic pyrolysis bio-oils by high-resolution techniques: 1 H NMR, GC × GC-TOFMS and FT-ICR MS. *J. Anal. Appl. Pyrolysis* 2016, *117*, 257–267.

(50) Huba, A. K.; Huba, K.; Gardinali, P. R. Understanding the atmospheric pressure ionization of petroleum components: The effects of size, structure, and presence of heteroatoms. *Sci. Total Environ.* 2016, *568*, 1018–1025.

(51) Gaspar, A.; Zellermann, E.; Lababidi, S.; Reece, J.; Schrader, W. Impact of different ionization methods on the molecular assignments of asphaltenes by FT-ICR mass spectrometry. *Anal. Chem.* 2012, *84*, 5257–5267.

(52) Chacón-Patiño, M. L.; Rowland, S. M.; Rodgers, R. P. The Compositional and Structural Continuum of Petroleum from Light Distillates to Asphaltenes: The Boduszynski Continuum Theory As Revealedby FT-ICR Mass Spectrometry. In *The Boduszynski continuum: Contributions to the understanding of the molecular composition of petroleum*; Ovalles, C., Moir, M. E., Eds.; ACS Symposium Series 1282; American Chemical Society: Washington DC, 2018; pp 113–171.

(53) McKenna, A. M.; Blakney, G. T.; Xian, F.; Glaser, P. B.; Rodgers, R. P.; Marshall, A. G. Heavy Petroleum Composition. 2. Progression of the Boduszynski Model to the Limit of Distillation by Ultrahigh-Resolution FT-ICR Mass Spectrometry. *Energy Fuels* 2010, *24*, 2939–2946.

(54) McKenna, A. M.; Purcell, J. M.; Rodgers, R. P.; Marshall, A. G. Heavy Petroleum Composition. 1. Exhaustive Compositional Analysis of Athabasca Bitumen HVGO Distillates by Fourier Transform Ion Cyclotron Resonance Mass Spectrometry: A Definitive Test of the Boduszynski Model. *Energy Fuels* 2010, *24*, 2929–2938.

(55) Ovalles, C.; Moir, M. E., Eds. *The Boduszynski continuum: Contributions to the understanding of the molecular composition of petroleum*; ACS Symposium Series 1282; American Chemical Society: Washington DC, 2018.

(56) Boduszynski, M. M.; Altgelt, K. H. Composition of heavy petroleums. 4. Significance of the extended atmospheric equivalent boiling point (AEBP) scale. *Energy Fuels* 1992, *6*, 72–76.

(57) ASTM D2892-18. *Test Method for Distillation of Crude Petroleum (15-Theoretical Plate Column)*; ASTM International: West Conshohocken, PA.

(58) Rüger, C. P.; Miersch, T.; Schwemer, T.; Sklorz, M.; Zimmermann, R. Hyphenation of Thermal Analysis to Ultrahigh-Resolution Mass Spectrometry (Fourier Transform Ion Cyclotron Resonance Mass Spectrometry) Using Atmospheric Pressure Chemical Ionization For Studying Composition and Thermal Degradation of Complex Materials. *Anal. Chem.* 2015, *87*, 6493–6499.

(59) Zhang, L.; Zhang, Y.; Zhao, S.; Xu, C.; Chung, K. H.; Shi, Q. Characterization of heavy petroleum fraction by positive-ion electrospray ionization FT-ICR mass spectrometry and collision induced dissociation: Bond dissociation behavior and aromatic ring architecture of basic nitrogen compounds. *Sci. China Chem.* 2013, *56*, 874–882.

(60) Qian, K.; Edwards, K. E.; Mennito, A. S.; Freund, H.; Saeger, R. B.; Hickey, K. J.; Francisco, M. A.; Yung, C.; Chawla, B.; Wu, C.*; et al.* Determination of structural building blocks in heavy petroleum systems by collision-induced dissociation Fourier transform ion cyclotron resonance mass spectrometry. *Anal. Chem.* 2012, *84*, 4544–4551.

(61) Mikhailenko, P.; Webber, G.; Baaj, H. Evaluation of solvents for asphalt extraction. *Road Mater. Pavement Des.* 2019, 1–12.

(62) Käfer, U.; Gröger, T.; Rohbogner, C. J.; Struckmeier, D.; Saraji-Bozorgzad, M. R.; Wilharm, T.; Zimmermann, R. Detailed Chemical Characterization of Bunker Fuels by High-Resolution Time-of-Flight Mass Spectrometry Hyphenated to GC × GC and Thermal Analysis. *Energy Fuels* 2019, *33*, 10745–10755.

(63) Jennerwein, M. K.; Eschner, M.; Gröger, T.; Wilharm, T.; Zimmermann, R. Complete Group-Type Quantification of Petroleum Middle Distillates Based on Comprehensive Two-Dimensional Gas Chromatography Time-of-Flight Mass Spectrometry (GC×GC-TOFMS) and Visual Basic Scripting. *Energy Fuels* 2014, *28*, 5670–5681.

(64) Weir, J. B. Significance of the Difference between Two Means when the Population Variances may be Unequal. *Nature* 1960, *187*, 438.

(65) Marshall, A. G.; Rodgers, R. P. Petroleomics: chemistry of the underworld. *Proc. Natl. Acad. Sci. U. S. A.* 2008, *105*, 18090–18095.

(66) Weggler, B. A.; Gröger, T.; Zimmermann, R. Advanced scripting for the automated profiling of two-dimensional gas chromatography-time-of-flight mass spectrometry data from combustion aerosol. *J. Chromatogr. A* 2014, *1364*, 241–248.

(67) Müller, H.; Andersson, J. T.; Schrader, W. Characterization of high-molecular-weight sulfur-containing aromatics in vacuum residues using Fourier transform ion cyclotron resonance mass spectrometry. *Anal. Chem.* 2005, *77*, 2536–2543.

(68) Lobodin, V. V.; Robbins, W. K.; Lu, J.; Rodgers, R. P. Separation and Characterization of Reactive and Non-Reactive Sulfur in Petroleum and Its Fractions. *Energy Fuels* 2015, *29*, 6177–6186.

(69) Hughey, C. A.; Rodgers, R. P.; Marshall, A. G.; Walters, C. C.; Qian, K.; Mankiewicz, P. Acidic and neutral polar NSO compounds in Smackover oils of different thermal maturity revealed by electrospray high field Fourier transform ion cyclotron resonance mass spectrometry. *Org. Geochem.* 2004, *35*, 863–880.

(70) Jarrell, T. M.; Jin, C.; Riedeman, J. S.; Owen, B. C.; Tan, X.; Scherer, A.; Tykwinski, R. R.; Gray, M. R.; Slater, P.; Kenttämaa, H. I. Elucidation of structural information achievable for asphaltenes via collision-activated dissociation of their molecular ions in MSn experiments: A model compound study. *Fuel* 2014, *133*, 106–114.

(71) Klein, G. C.; Kim, S.; Rodgers, R. P.; Marshall, A. G.; Yen, A. Mass Spectral Analysis of Asphaltenes. II. Detailed Compositional Comparison of Asphaltenes Deposit to Its Crude Oil Counterpart for Two Geographically Different Crude Oils by ESI FT-ICR MS. *Energy Fuels* 2006, *20*, 1973–1979.

(72) Porto, C. F.C.; Pinto, F. E.; Souza, L. M.; Madeira, N. C.L.; Neto, Á. C.; Menezes, S. M.C. de; Chinelatto, L. S.; Freitas, C. S.; Vaz, B. G.; Lacerda, V.*; et al.* Characterization of organosulfur compounds in asphalt cement samples by ESI(+)FT-ICR MS and 13C NMR spectroscopy. *Fuel* 2019, *256*, 115923.

(73) Qian, K.; Rodgers, R. P.; Hendrickson, C. L.; Emmett, M. R.; Marshall, A. G. Reading Chemical Fine Print: Resolution and Identification of 3000 Nitrogen-Containing Aromatic Compounds from a Single Electrospray Ionization Fourier Transform Ion Cyclotron Resonance Mass Spectrum of Heavy Petroleum Crude Oil. *Energy Fuels* 2001, *15*, 492–498.

(74) Zhu, X.; Shi, Q.; Zhang, Y.; Pan, N.; Xu, C.; Chung, K. H.; Zhao, S. Characterization of Nitrogen Compounds in Coker Heavy Gas Oil and Its Subfractions by Liquid Chromatographic Separation Followed by Fourier Transform Ion Cyclotron Resonance Mass Spectrometry. *Energy Fuels* 2011, *25*, 281–287.

(75) Chiron, J.; Galy, J.-P. Reactivity of the Acridine Ring: A Review. *Synthesis* 2004, 313–325.

(76) Mirwald, J.; Werkovits, S.; Camargo, I.; Maschauer, D.; Hofko, B.; Grothe, H. Understanding bitumen ageing by investigation of its polarity fractions. *Constr. Build. Mater.* 2020, *250*, 118809.

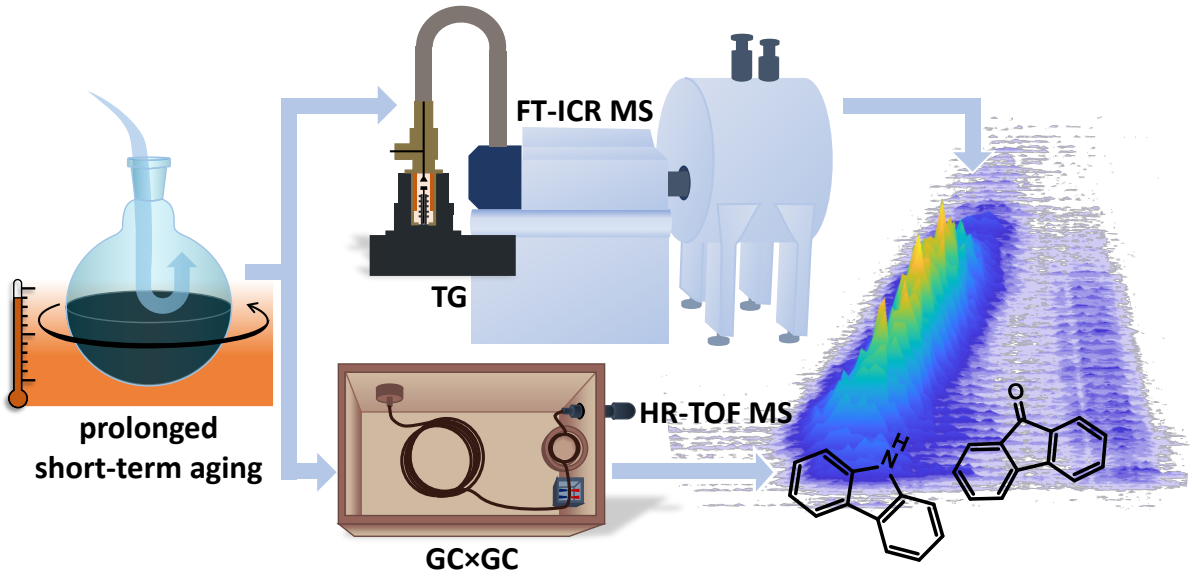

For table of content only.

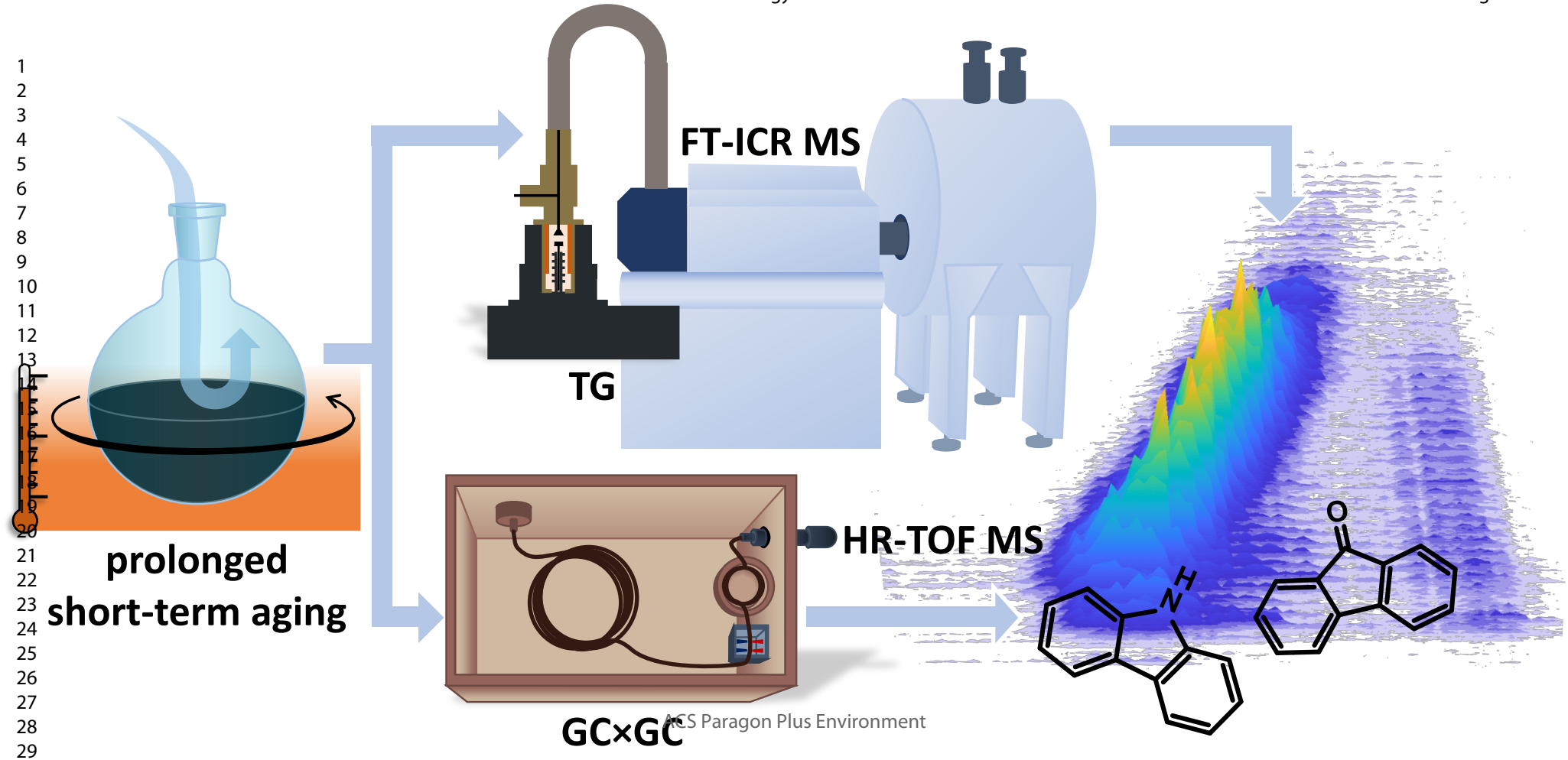
FT-ICR MS
TG
prolonged
short-term aging
HR-TOF MS
GC×GC

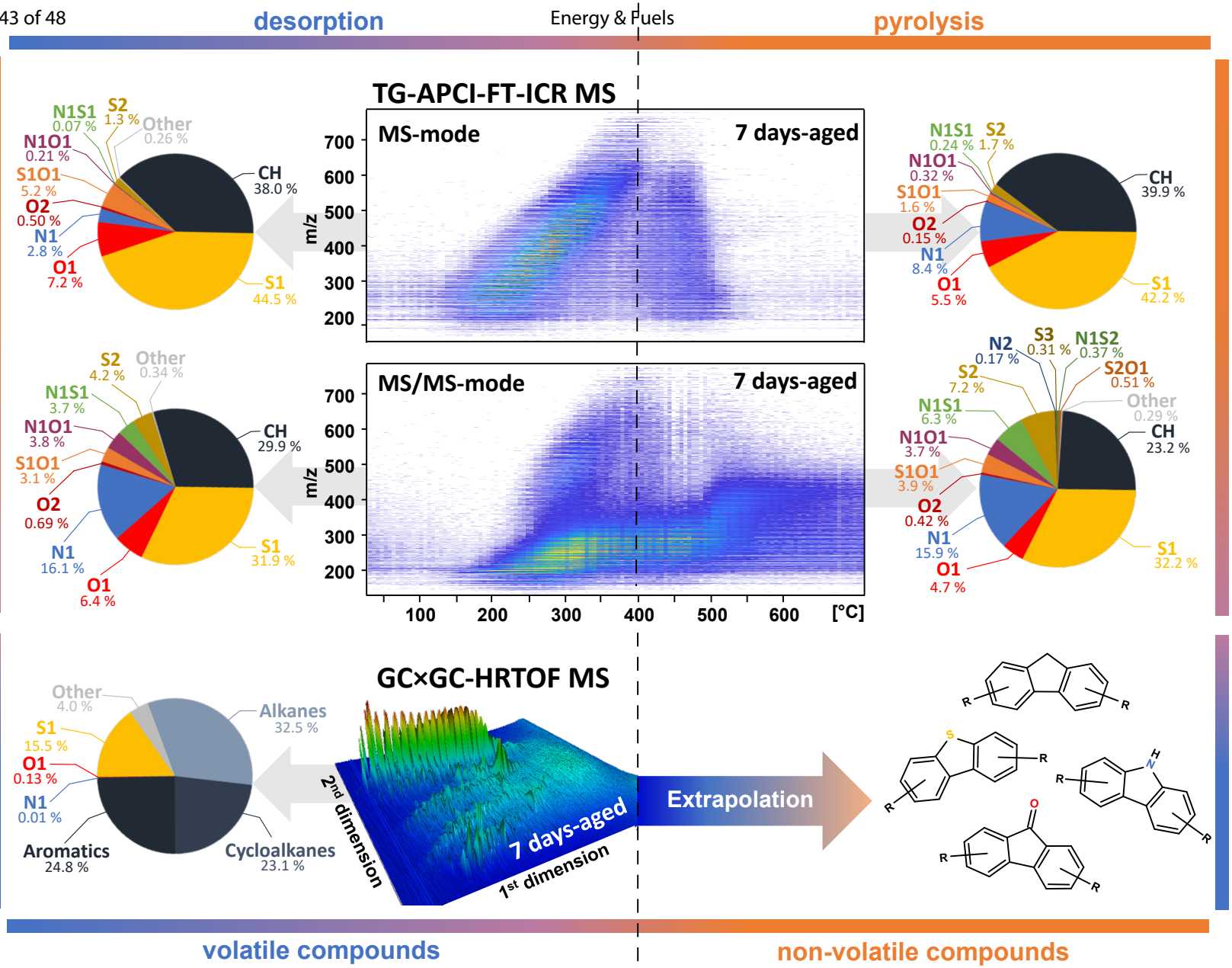

addressed by TG-APCI-FT-ICR MS

addressed by both methods

addressed by GC×GC-HRTOFMS

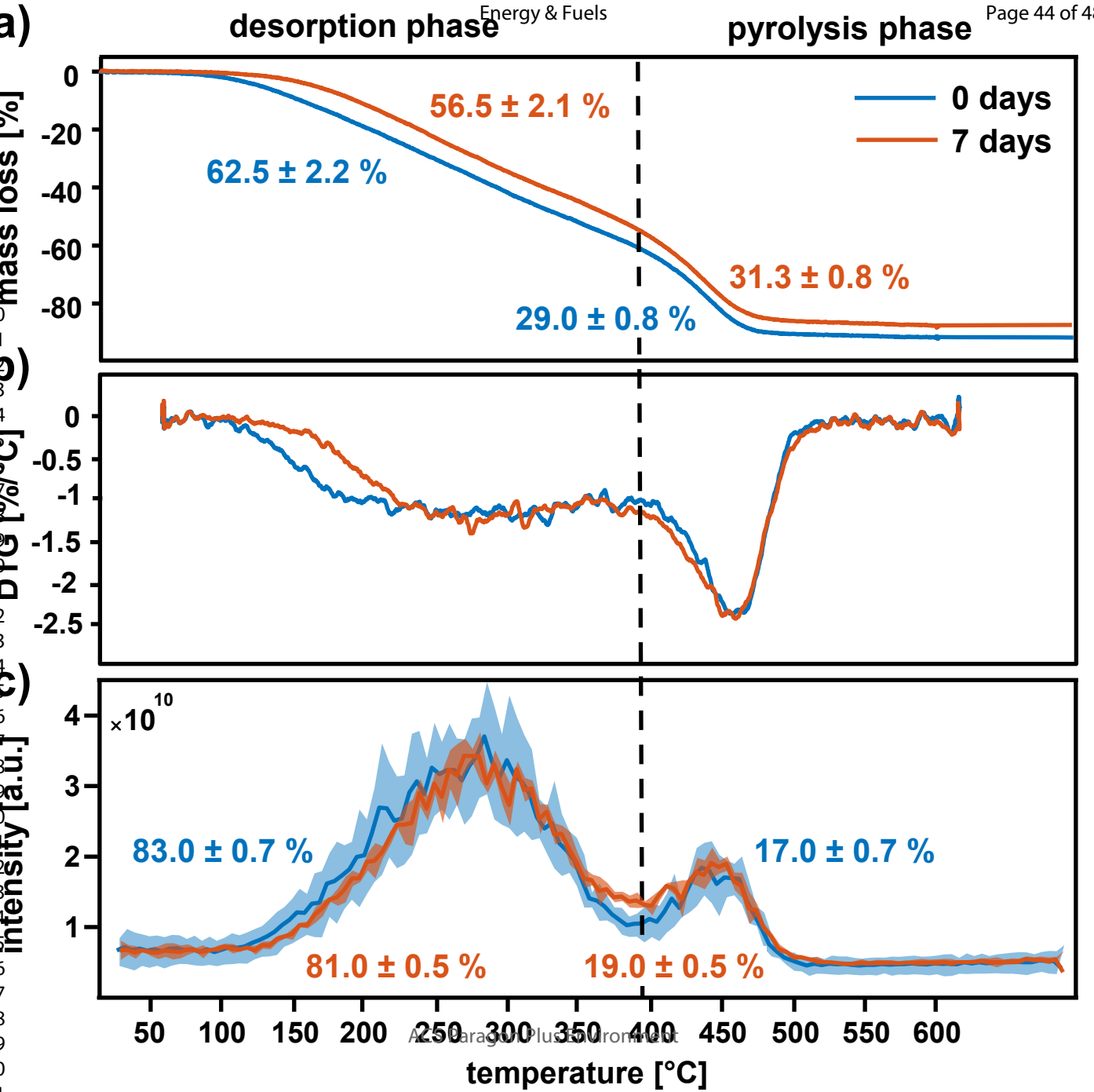

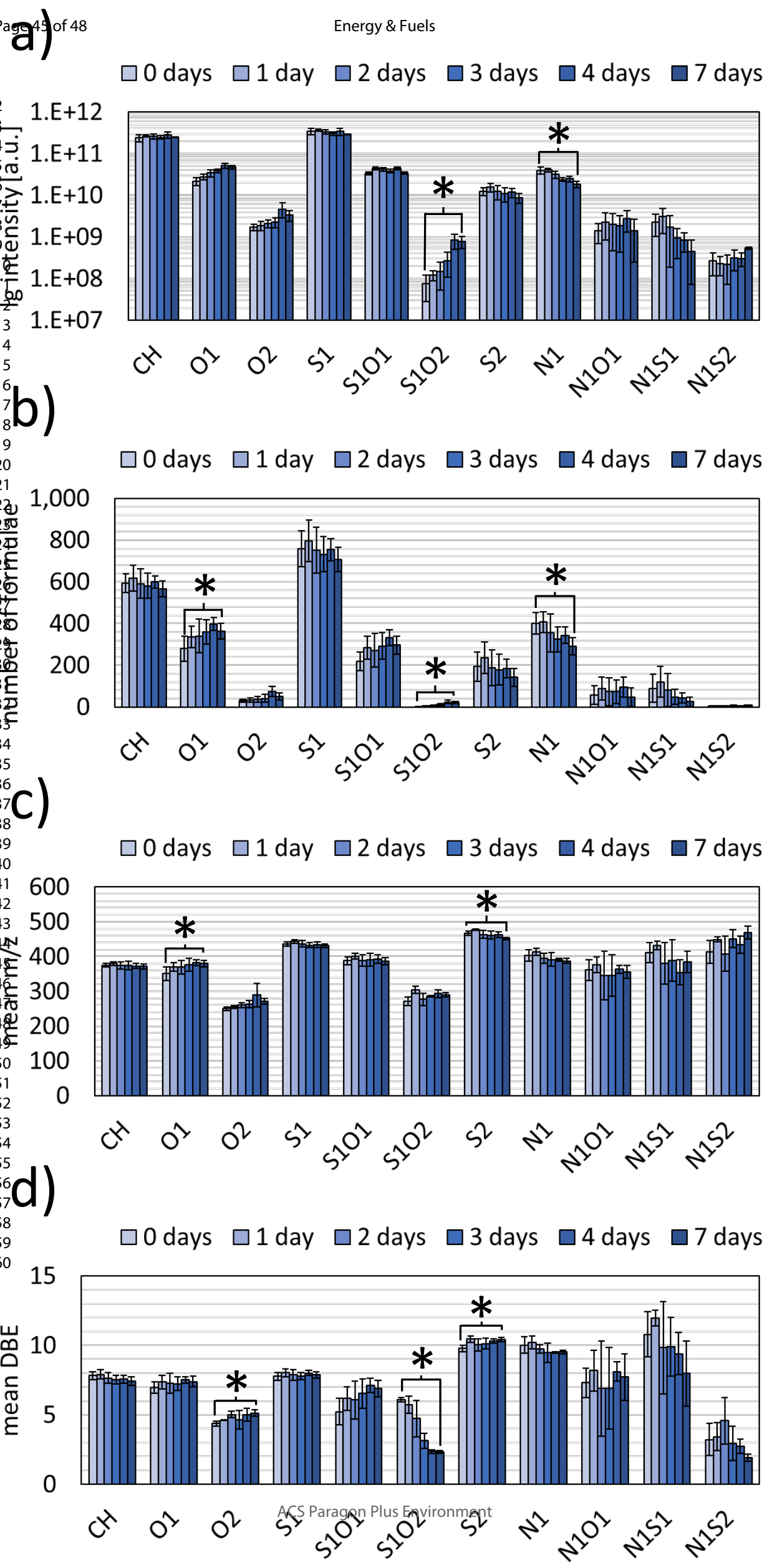
a)
0 days
1 day
2 days
3 days
4 days
7 days
1.E+12
1.E+11
1.E+10
1.E+09
1.E+08
1.E+07
Intensity [a.u.]
*
*
*
CH
O1
O2
S1
S1O1
S1O2
S2
N1
N1O1
N1S1
N1S2
b)
0 days
1 day
2 days
3 days
4 days
7 days
1,000
800
600
400
200
0
number of formulae
*
*
*
CH
O1
O2
S1
S1O1
S1O2
S2
N1
N1O1
N1S1
N1S2
c)
0 days
1 day
2 days
3 days
4 days
7 days
600
500
400
300
200
100
0
mean m/z
*
*
*
CH
O1
O2
S1
S1O1
S1O2
S2
N1
N1O1
N1S1
N1S2
d)
0 days
1 day
2 days
3 days
4 days
7 days
15
10
5
0
mean DBE
*
*
*
*
CH
O1
O2
S1
S1O1
S1O2
S2
N1
N1O1
N1S1
N1S2

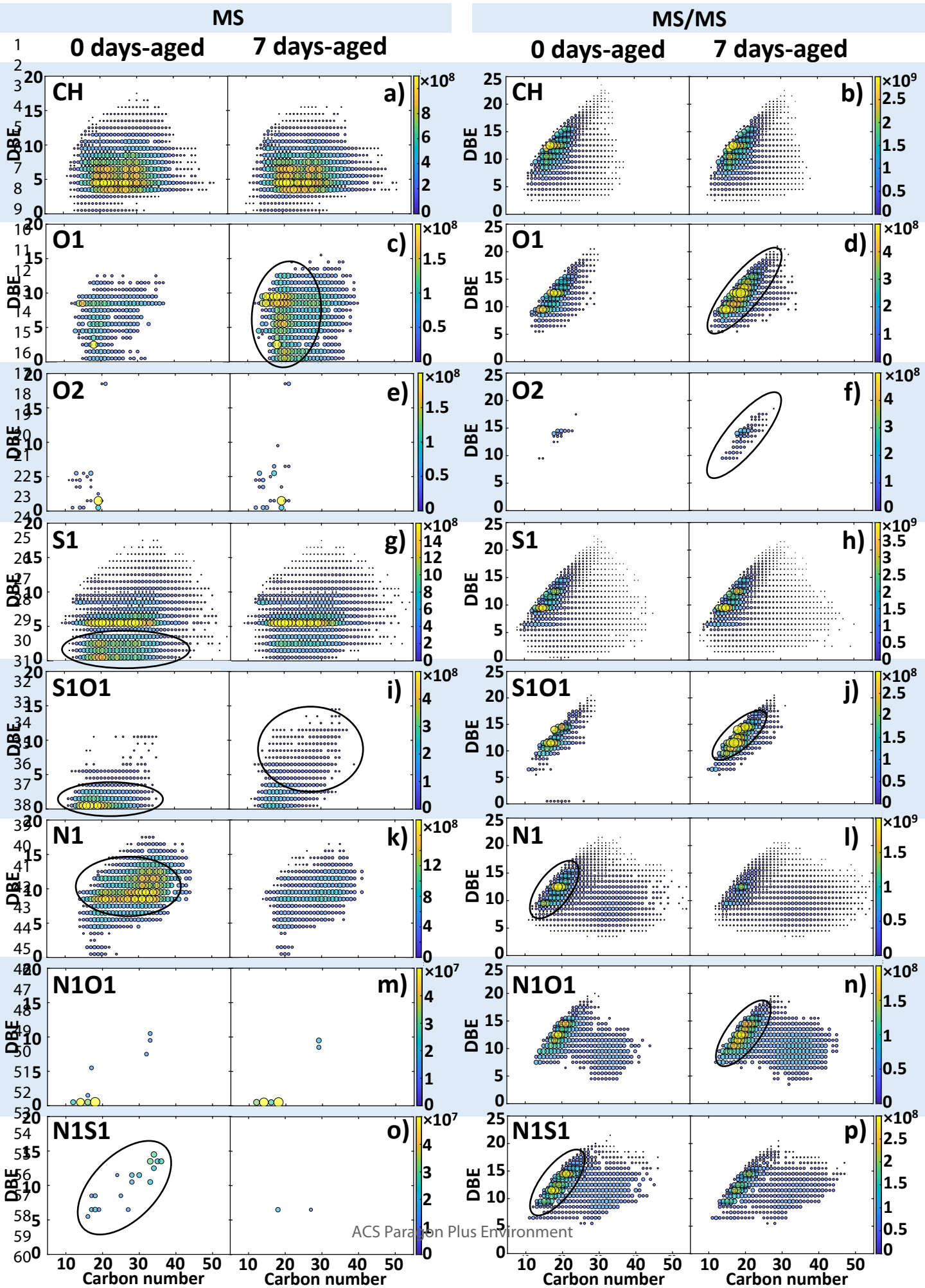
MS
MS/MS
0 days-aged
7 days-aged
0 days-aged
7 days-aged
CH
a)
CH
b)
O1
c)
O1
d)
O2
e)
O2
f)
S1
g)
S1
h)
S1O1
i)
S1O1
j)
N1
k)
N1
l)
N1O1
m)
N1O1
n)
N1S1
o)
N1S1
p)
DBE
Carbon number
Carbon number
Carbon number
Carbon number

Pyrolysis phase

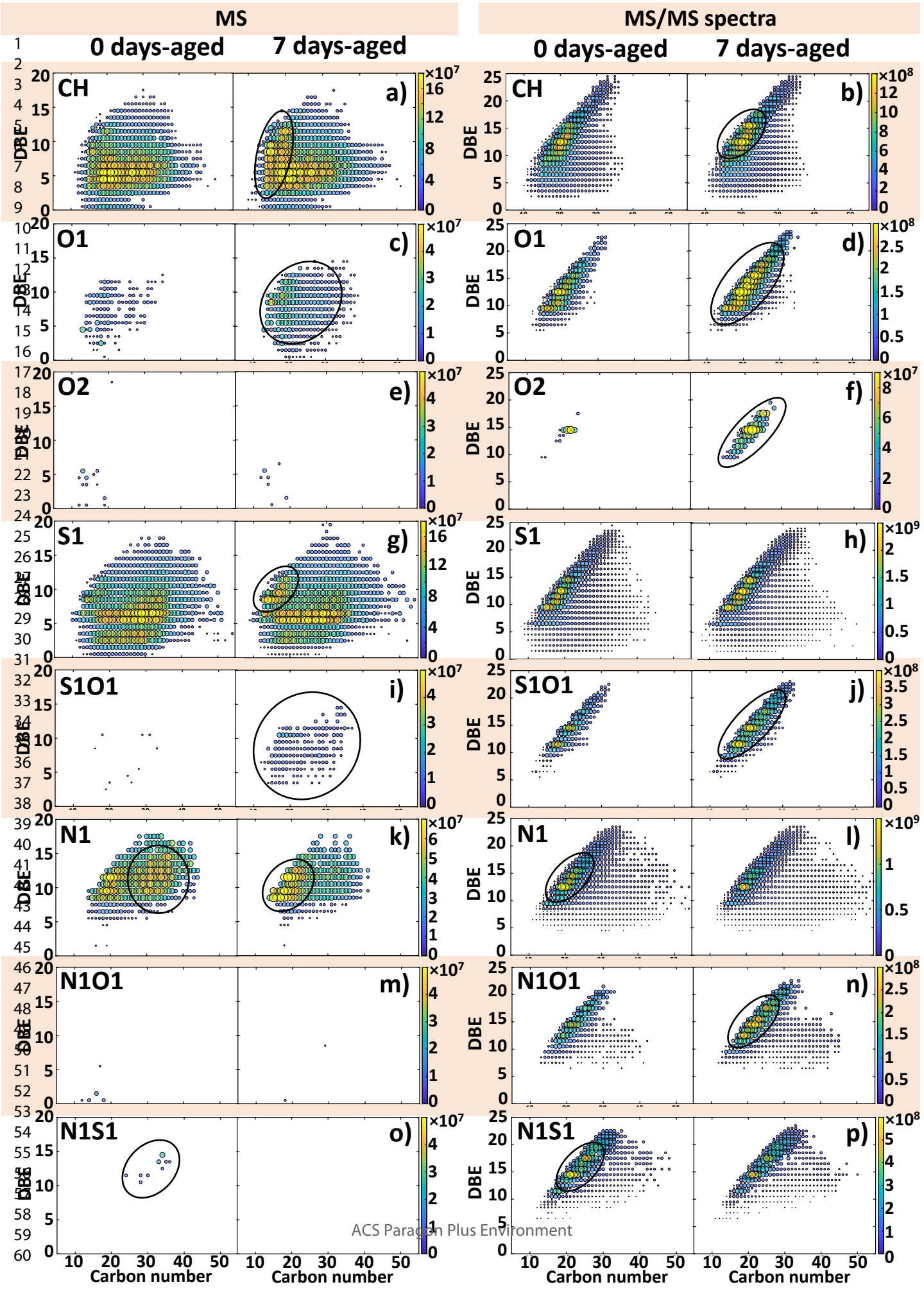

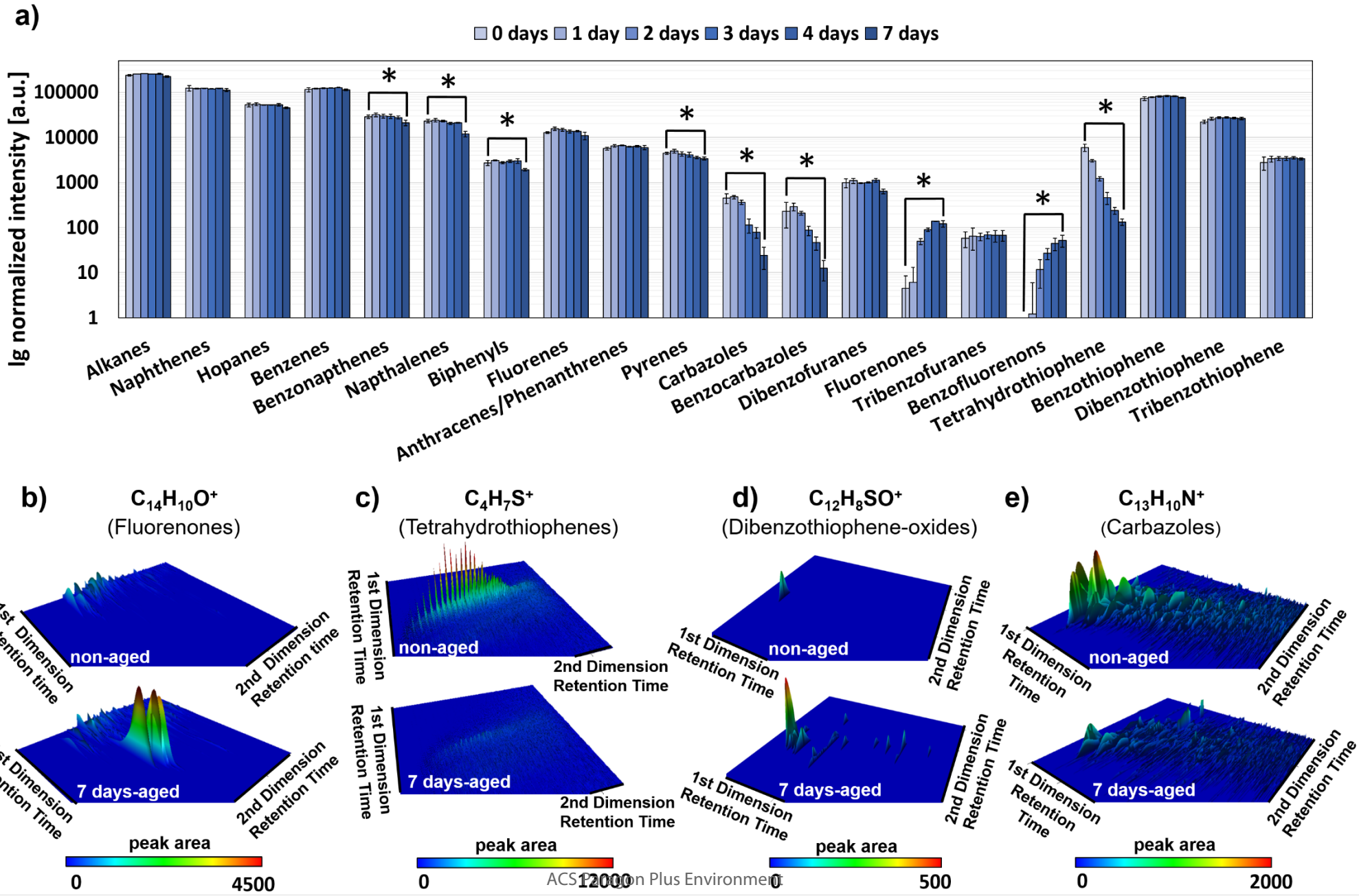
a)
0 days 1 day 2 days 3 days 4 days 7 days
lg normalized intensity [a.u.]
100000
10000
1000
100
10
1
*
Alkanes
Naphthenes
Hopanes
Benzenes
Benzonapthenes
Napthalenes
Biphenyls
Fluorenes
Anthracenes/Phenanthrenes
Pyrenes
Carbazoles
Benzocarbazoles
Dibenzofuranes
Fluorenones
Tribenzofuranes
Benzofluorenons
Tetrahydrothiophene
Benzothiophene
Dibenzothiophene
Tribenzothiophene
b)
$C_{14}H_{10}O^+$
(Fluorenones)
non-aged
7 days-aged
1st Dimension Retention time
2nd Dimension Retention time
peak area
0
4500
c)
$C_4H_7S^+$
(Tetrahydrothiophenes)
non-aged
7 days-aged
1st Dimension Retention Time
2nd Dimension Retention Time
peak area
0
12000
d)
$C_{12}H_8SO^+$
(Dibenzothiophene-oxides)
non-aged
7 days-aged
1st Dimension Retention Time
2nd Dimension Retention Time
peak area
0
500
e)
$C_{13}H_{10}N^+$
(Carbazoles)
non-aged
7 days-aged
1st Dimension Retention Time
2nd Dimension Retention Time
peak area
0
2000